MICROBIOLOGY

Gut microbiota from patients with arteriosclerotic CSVD induces higher IL-17A production in neutrophils via activating RORγt

Wei Cai[1,2,3]*, Xiaodong Chen[1]*, Xuejiao Men[1], Hengfang Ruan[1], Mengyan Hu[1], Sanxin Liu[1], Tingting Lu[1], Jinchi Liao[1], Bingjun Zhang[1], Danli Lu[1], Yinong Huang[1], Ping Fan[1], Junping Rao[4], Chunyan Lei[5], Jihui Wang[6], Xiaomeng Ma[1], Qiang Zhu[1], Lili Li[1], Xiuyun Zhu[1], Yujiao Hou[4], Shu Li[4], Qing Dong[1], Qing Tian[1], Lulu Ai[1], Wenjing Luo[1], Mengyun Zuo[1], Liping Shen[1], Congyan Xie[1], Hongzhong Song[4], Ganlin Xu[5], Kangdi Zheng[5], Zhao Zhang[5], Yongjun Lu[7], Wei Qiu[1], Tao Chen[5,8], Andy Peng Xiang[1,3]†, Zhengqi Lu[1]†

The intestinal microbiota shape the host immune system and influence the outcomes of various neurological disorders. Arteriosclerotic cerebral small vessel disease (aCSVD) is highly prevalent among the elderly with its pathological mechanisms yet is incompletely understood. The current study investigated the ecology of gut microbiota in patients with aCSVD, particularly its impact on the host immune system. We reported that the altered composition of gut microbiota was associated with undesirable disease outcomes and exacerbated inflammaging status. When exposed to the fecal bacterial extracts from a patient with aCSVD, human and mouse neutrophils were activated, and capacity of interleukin-17A (IL-17A) production was increased. Mechanistically, RORγt signaling in neutrophils was activated by aCSVD-associated gut bacterial extracts to up-regulate IL-17A production. Our findings revealed a previously unrecognized implication of the gut-immune-brain axis in aCSVD pathophysiology, with therapeutic implications.

INTRODUCTION

Cerebral small vessel disease (CSVD) is a subset of disorders that involves malfunction of small arteries, arterioles, capillaries, and small veins in the brain (*1*). As life expectancy keeps increasing globally, CSVD, which is highly prevalent among senile population, has displayed severe consequences. Mounting evidence indicates the role of CSVD in promoting neurodegeneration and worsening the symptoms (*2*). It is documented that CSVD contributes to ~45% of dementia cases worldwide (*3*). CSVD increases the risk of acute cerebral vascular events. Approximately one-quarter of all strokes could be attributed to CSVD (*3*). Arteriosclerotic CSVD (aCSVD) is one of the major subtypes of the CSVD spectrum. During the development of aCSVD, small vessels in the brain undergo accumulated injuries due to genetic factors, environmental factors, or both (*4*, *5*). The course of the disease starts silently and progresses gradually over time before the emergence of notable symptoms. The lengthy pathophysiological process complicates the pathogenesis of aCSVD, which further toughens the therapeutic research. Nowadays, our knowledge on aCSVD development remains to be superficial, and the therapeutic countermeasures are limited.

The role of chronic systemic inflammation in aCSVD pathophysiology has only recently been recognized (*6*–*9*). Systemic and vascular inflammatory status have been found to be associated with aCSVD development and prognosis (*1*). The peripheral immune system, including both the innate and adaptive immune cells, plays a crucial role in the pathophysiology of aCSVD. Infiltration of neutrophils through the blood-brain barrier (BBB) into aCSVD lesions and their continuous release of BBB destroying matrix metalloproteinase-9 (MMP9) have been identified (*9*). Increased cytokine production capacity of circulating monocytes in patients with aCSVD has been recorded (*7*). Release of central nervous system (CNS) antigen into the peripheral circulation results in development and activation of CNS antigen–specific lymphocytes (*10*, *11*). Multiple inflammatory mediators derived from the activated immune cells contribute to aCSVD development. Systemic inflammatory factors [e.g., C-reactive protein, interleukin-6 (IL-6), tumor necrosis factor–α (TNFα), myeloperoxidase] and vascular inflammatory factors [e.g., homocysteine, intracellular adhesion molecule-1 (ICAM-1), vascular cell adhesion molecule-1 (VCAM-1)] synergistically drive the progression of small vessel pathology (*1*). Tackling the immune reactions that injure the brain endothelium and BBB could be a promising therapeutic strategy.

The continuous interaction between gut microbiota and the host immune system has a vital impact on the induction, functional modulation, or suppression of local and systemic immune responses (*12*). It is reported that acute ischemic stroke–associated gut microbiota facilitate the expansion of IL-17A–producing T cells, which exacerbates poststroke neural inflammation. Loss of microbiota diversity in the gut is proved to be associated with the increased formation of

[1]Department of Neurology, Mental and Neurological Disease Research Center, the Third Affiliated Hospital of Sun Yat-sen University, Guangzhou 510630, China. [2]Center of Clinical Immunology, Mental and Neurological Disease Research Center, the Third Affiliated Hospital of Sun Yat-sen University, Guangzhou 510630, China. [3]Center for Stem Cell Biology and Tissue Engineering, Key Laboratory for Stem Cells and Tissue Engineering, Ministry of Education, Sun Yat-Sen University, Guangzhou 510080, China. [4]Department of Neurology, Yuedong Hospital, the Third Affiliated Hospital of Sun Yat-sen University, Meizhou, Guangdong 514011, China. [5]South China Institute of Biomedicine, Guangzhou, Guangdong 510535, China. [6]Department of Psychiatry, the Third Affiliated Hospital of Sun Yat-sen University, Guangzhou, Guangdong 510630, China. [7]Run Ze Laboratory for Gastrointestinal Microbiome Study, School of Life Sciences and Biomedical Center of Sun Yat-sen University, Guangzhou, Guangdong 510275, China. [8]Center of Human Microecology Engineering and Technology of Guangdong Province, Guangzhou, Guangdong 510535, China.
*These authors contributed equally to this work.
†Corresponding author. Email: lzq1828@outlook.com (Z.L.); xiangp@mail.sysu.edu.cn (A.P.X.)

neutrophil extracellular traps (NETs) (*13*). A microbial product, trimethylamine *N*-oxide (TMAO), is associated with excessive local and systemic inflammatory mediators, altered intestinal permeability, and increased circulating bacterial DNA, which may facilitate the development of aging-related coronary arteriosclerosis (*14*). Accumulating evidence has shown that alteration of the gut microbiota is one of the potential mechanisms of age-related chronic inflammatory status, which is called "inflammaging" (*15*). We thus inferred that the pace of inflammaging in patients with aCSVD, the majority of whom are elderly persons, could be modified by gut microbiota. Nevertheless, the ecology of the gut microbiota in patients with aCSVD has not been characterized. How the intestinal microbiota shape the immune system and promote the pathophysiological process of aCSVD remains elusive.

In the current study, we investigated the features of commensal microbiota in patients with aCSVD, the impact of altered intestinal microbiota on the immune system, and the influence of the gut-immune axis on aCSVD prognosis. We aim at providing valuable hints to the understanding of aCSVD pathophysiology, early recognition, and alertness of undesirable disease outcomes, as well as the corresponding therapeutic countermeasures.

RESULTS

Diversity of intestinal microbiota increases in patients with aCSVD

Interaction of the gut microbiota, inflammaging status, and aCSVD pathophysiology in the cohort was investigated. The study design is displayed in Fig. 1A. Fecal samples of 55 patients with aCSVD [mean age, 65.42 ± 7.78 years; male, 36 (58.06%); 30 with burden = 0 to 1, 25 with burden = 2 to 4] were collected and subjected to r16*S* sequencing. Magnetic resonance imaging (MRI) scanning and Montreal cognitive assessment (MoCA) were performed to the recruited patients to evaluate aCSVD severity. A total of 62 age-matched healthy controls [HCs; mean age, 64.84 ± 9.35 years; male, 33 (60.00%)] were recruited and donated their fecal samples to the study. The process of exclusion and inclusion is displayed in fig. S1. Clinical characteristics of the cohort, including demographic and laboratory biomedical factors, are shown in table S1. In the cohort, mRNA was extracted from the total peripheral blood leukocytes of 31 HCs and 38 patients with aCSVD (20 with burden = 0 to 1, 18 with burden = 2 to 4) and was subjected to inflammaging status analysis. Clinic characteristics of the 69 individuals are displayed in table S2.

Taxonomic classification of the cohort gut community revealed 109 genera from 12 major phyla (fig. S2, A and B). Relative abundance of gut microbiota (>10^{-5}) at the genus level of the cohort is displayed (Fig. 1B; legends are shown in fig. S2C). In HCs, the top 10 genera with the highest relative abundance in gut microbiota were g_Lachnospira, g_Bilophila, g_Clostridium, g_Haemophilus, g_Dialister, g_Veillonella, g_Granulicatella, g_Dorea, g_Desulfovibrio, and g_Akkermansia. In patients with aCSVD, the 10 genera that were most predominant in gut microbiota were g_Bacteroides, g_Faecalibacterium, g_Escherichia, g_Roseburia, g_Lachnospira, g_Parabacteroides, g_Streptococcus, g_Megamonas, g_Oscillospira, and g_Ruminococcus. In comparing α-diversity in the cohort (N = 117), we found that the gut microbiota of patients with aCSVD with burden = 2 to 4 had higher Chao1 richness, observed operational taxonomic unit (OTU), and Faith's phylogenetic diversity (PD). Accordingly, their Pielou E value decreased. The gut microbiota of HCs and patients with aCSVD showed consistent values in the analysis of Shannon-Wiener diversity index and Simpson diversity index (Fig. 1C). β-Diversity of the cohort was assessed with partial least squares discriminant analysis (PLS-DA) (fig. S2D). Overall, our data indicated that intestinal microbiota of patients with aCSVD showed higher diversity compared with their healthy contemporary.

Composition of gut commensal microbiota of patients with aCSVD differs from that of the HCs

To depict the characteristics of gut microbiota in the cohort, we performed assessment of the linear discriminant analysis (LDA) effect size (LEfSe) (Fig. 1D). Distinctive gut microbiota taxa with LDA score >2 from the level of phylum to species (Fig. 1D) and their phylogenetic taxonomy (Fig. 1E) are displayed. In gut microbiota of patients with aCSVD, expansion of bacterial members in p_Proteobacteria, p_Actinobacteria, p_Firmicutes, p_Bacteroidetes, p_Cyanobacteria, and p_TM7 was detected (Fig. 1, D and E). The genus composition with LDA score >2 in LEfSe analysis displayed notable difference between HCs and patients with aCSVD (Fig. 1, F and G, and fig. S2E). For example, abundance of g_Escherichia was significantly higher in gut microbiota of patients with aCSVD, and the patients with aCSVD burden = 2 to 4 borne more g_Escherichia in their gut microbiota compared with patients with aCSVD burden = 0 to 1 (Fig. 1G and fig. S2E). With Spearman correlation analysis, we found close interactions among the gut commensal bacterial populations at all taxonomic levels (fig. S3). Our data support the idea that the gut commensal microbiota system functions and affects the pathophysiology of various diseases as a whole (*16*).

Alteration of gut microbiota in patients with aCSVD correlates with neuroimaging markers and MoCA, which displays early alarming value

We next evaluated the clinical significance of the altered intestinal microbiota in aCSVD pathophysiology. The association of altered gut microbiota with clinical indications was assessed with Spearman correlation matrix analysis. Gut microbiota with LDA score >2 was included in the assessment. The corresponding neuroimaging markers of aCSVD accessed with MRI in patients, including lacunae, deep-white matter hyperintensities (d-WMH), periventricular-WMH (p-WMH), lobar cerebral microbleeds (CMBs) and deep/infratentorial CMBs, perivascular space (PVS) in basal ganglia (BG) and centrum semiovale, cerebral atrophy, and the total aCSVD burden, were evaluated in the analysis. The value of MoCA was also included in the correlation evaluation. We found that the altered microbiota composition had considerable impacts on the imageology of patients with aCSVD. As an example, WMH, the most important imaging biomarker of aCSVD, was positively correlated with the relative abundance of p_Proteobacteria (Fig. 2A). Representative magnetic resonance (MR) images of typical patients with aCSVD and their corresponding microbiota composition (genus level, LDA score >2) are displayed (Fig. 2Bb). The multiple injuries of brain vessels are usually irreversible in aCSVD. Consequently, early recognition of disease status and alertness of undesirable prognosis are of importance. To evaluate the value of microbiota alteration as an early clinical alarm for detrimental aCSVD outcomes, we divided the patients into two groups according to their radiological burden: mild aCSVD (burden = 0 to 1) and moderate-severe aCSVD (burden = 2 to 4). Epidemiological characteristics of the patients with aCSVD, with or without the composition of microbiota (defined as

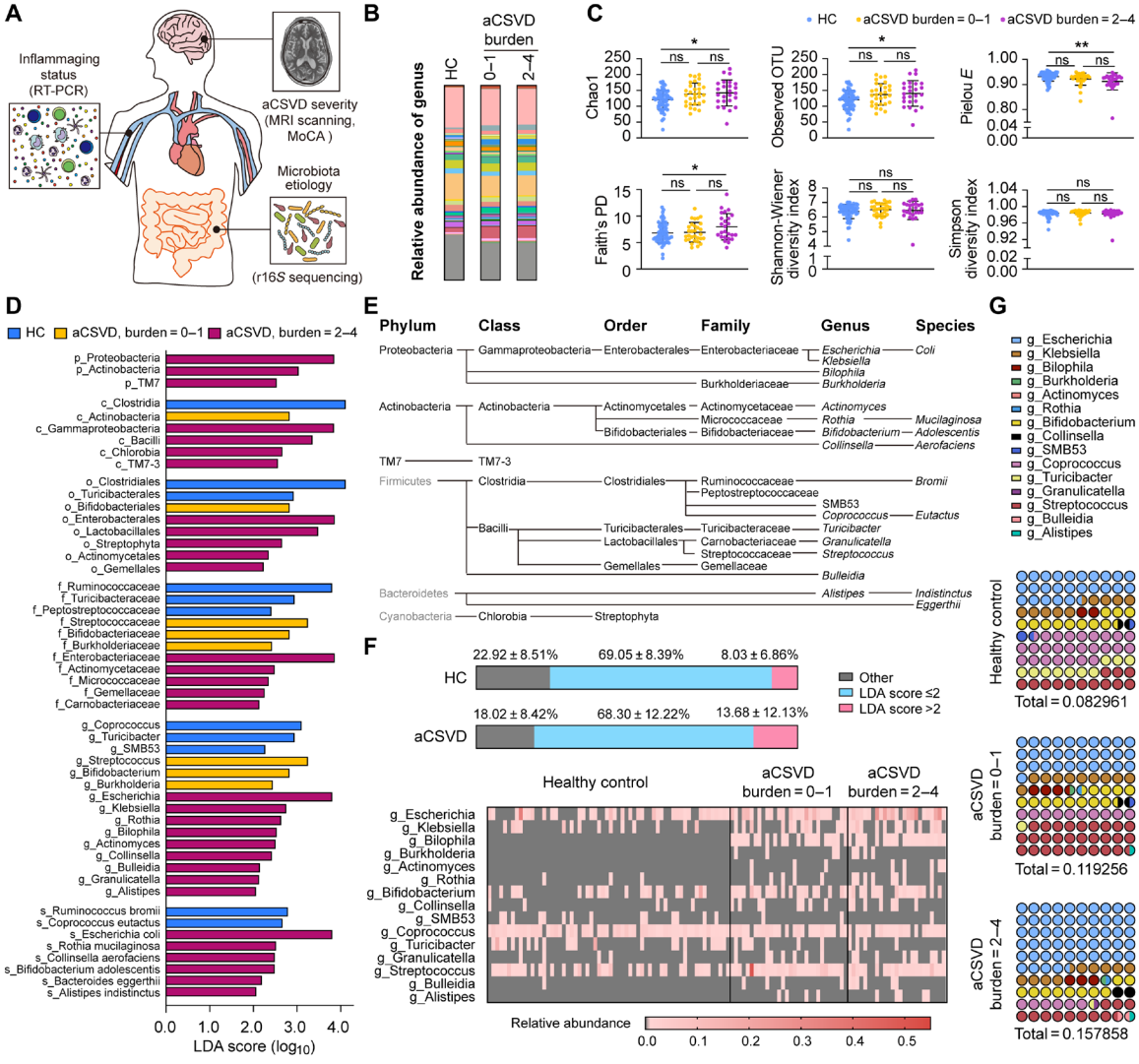

Fig. 1. Gut microbiota composition of patients with aCSVD and HCs. (**A**) Experimental design. (**B**) Stacked graph depicting composition of bacterial genera with relative abundance >10^{-5} in the cohort. Legends are displayed in fig. S2C. (**C**) Diversity analysis of gut microbiota of the whole cohort. *$P < 0.05$; **$P < 0.01$; ns, $P \geq 0.05$; by one-way analysis of variance (ANOVA) (mean ± SD). (**D**) Characteristics of gut microbiota in the cohort were evaluated with LEfSe. Bacterial populations with LDA score >2 are displayed. (**E**) Phylogenetic classification of bacterial populations with LDA score >2. The subordinate phylum with LDA score ≤2 is displayed with gray characters. (**F**) Top: Frequencies of the gut bacterial genera according to LDA score. Mean ± SE is displayed. Bottom: Heatmap illustrating the relative abundance of gut bacterial genera with LDA score >2 in patients with aCSVD and HCs. (**G**) Dot plot (10 × 10) depicting the weight distribution of the 15 genera with LDA score >2. The value of "Total" indicated the proportion of the 15 genera with LDA score >2 among the whole gut microbiota (total = 1). Comparison of the relative abundance of the 15 genera with LDA score >2 among the three subgroups with one-way ANOVA is displayed in fig. S2E.

the relative abundance of bacterial genera in gut microbiota with LDA score >2), were subjected to receiver operating characteristic (ROC) analysis. The epidemiological parameters alone, namely, age, body mass index (BMI), smoking behavior, and comorbidity of hypertension and diabetes, had made considerable contribution to prediction efficacy of detrimental aCSVD imageology (burden = 2 to 4) with an area under curve (AUC) of 71.33 ± 6.98% ($P = 0.0068$). Notably, when the relative abundance of the gut bacterial genera with LDA score >2 was incorporated into the model construction, the AUC increased to 88.00 ± 4.53% ($P < 0.0001$) (Fig. 2C). Our data indicated that the relative abundance of the 15 genera with LDA score >2 identified in our cohort was of important alarming value in aCSVD prognosis.

Alteration in gut microbiota of patients with aCSVD is associated with the increased pace of inflammaging

We next investigated how the altered microbiota affected aCSVD pathophysiology according to the study design (Fig. 1A). aCSVD is most prevalent among the elderly. Age-related dishomeostasis of the immune system, designated as inflammaging, is associated with various neurological disorders (*17*). It is evident that intestinal dysbiosis promotes inflammaging during aging (*18*). Therefore, we hypothesized that the altered microbiota in patients with aCSVD accelerated the process of inflammaging, which exacerbated aCSVD pathophysiology. We first evaluated the systemic inflammatory status of patients with aCSVD by measuring the mRNA level of inflammaging markers (*19*) in circulating leukocytes with real-time polymerase chain reaction

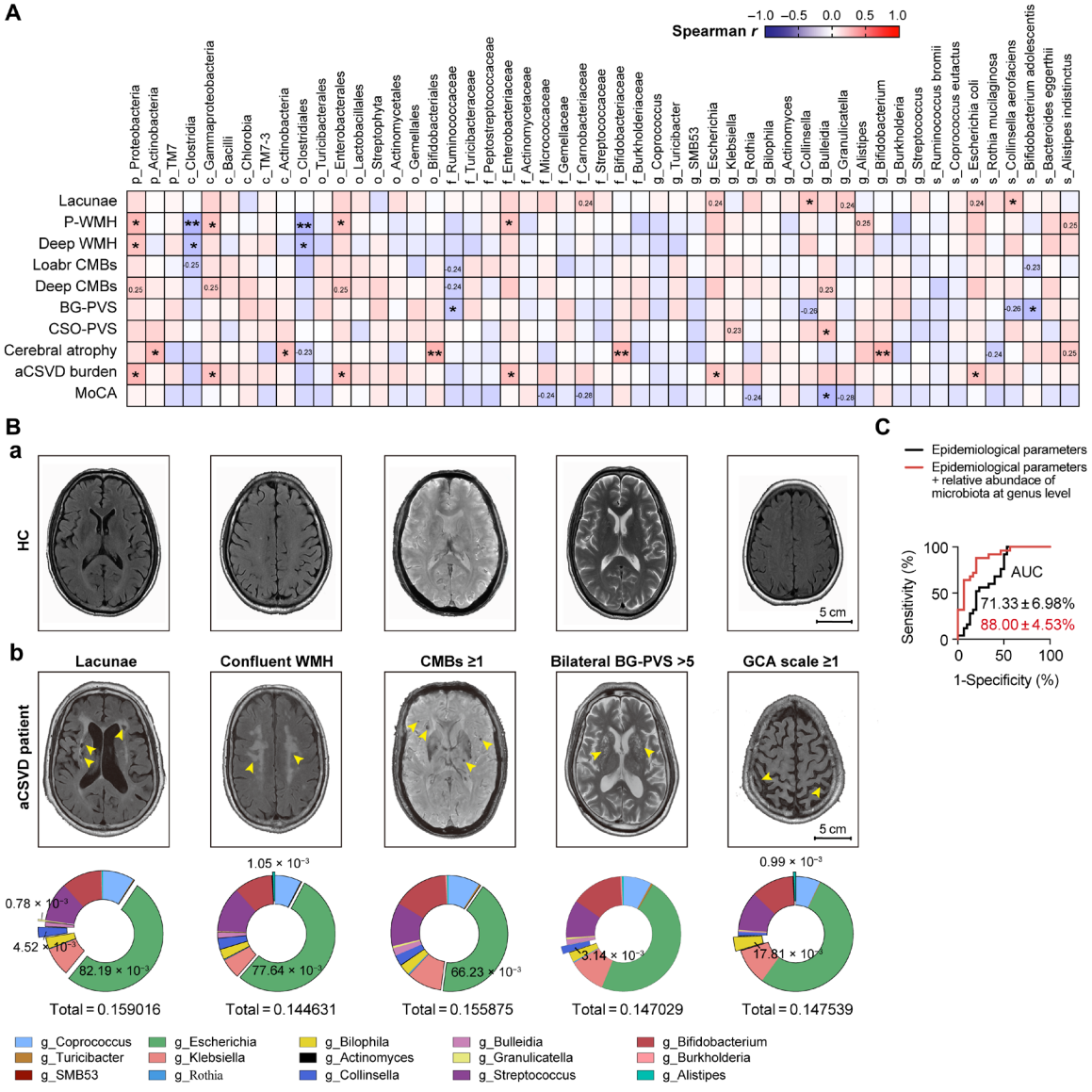

Fig. 2. Association of gut microbiota and clinical manifestations of patients with aCSVD. (**A**) Association of the altered bacterial composition and the clinical indications was evaluated with Spearman correlation analysis. $N = 30$ in patients with aCSVD with burden = 0 to 1, and $N = 25$ in patients with aCSVD with burden = 2 to 4. *$P < 0.05$ and **$P < 0.01$. The r values ~0.25 are also displayed. (**B**) Representative MR images of HC (**a**) and typical patients with aCSVD together with their corresponding microbiota composition (weight of genera with LDA score >2) (**b**). Yellow arrowheads emphasize the indicated MRI signs. (**C**) Graph depicts the results of the ROC analysis of predicting efficacy for detrimental imageology (aCSVD burden = 2 to 4). AUC of epidemiological characteristics (black curve, black characters; 71.33 ± 6.98%, $P = 0.0068$) and that in addition with the relative abundance of the 15 genera with LDA score >2 (red curve, red characters; 88.00 ± 4.53%, $P < 0.0001$) is displayed. $N = 30$ in patients with aCSVD with burden = 0 to 1, and $N = 25$ in patients with aCSVD with burden = 2 to 4.

(RT-PCR). We found that expression of the inflammaging markers *IL-17A*, *TNFα*, *IL-6*, and *IFNα* (*19*) increased in patients with aCSVD compared with their healthy counterparts (Fig. 3A and fig. S4), which revealed that the pace of inflammaging was advanced in patients with aCSVD. Among all the assessed inflammaging markers, mRNA expression of *IL-17A* had the largest difference of means (1.43 ± 0.4412) between the two groups, illustrating that *IL-17A* mRNA level displayed the most considerable alteration in patients with aCSVD (Fig. 3A). To address the prognostic value of the tested inflammaging markers, we incorporated their mRNA level in the ROC analysis for detrimental imageology signs (aCSVD burden = 2 to 4) together with the epidemiological parameters. Inclusion of the inflammaging markers in the ROC analysis increased the AUC to 83.06 ± 6.63% ($P = 0.0005$), indicating that the elevated inflammaging status displayed prognostic significance (Fig. 3B). Among the tested parameters, mRNA expression of *IL-1β*, *IL-6*, *IFNα*, and *IL-17A* increased the predicting sensitivity for detrimental imageology signs (aCSVD burden = 2 to 4) (Fig. 3C). To be noted, the AUC with *IL-6* (79.17 ± 7.22%, $P = 0.0021$) or *IL-17A* (79.17 ± 7.18%, $P = 0.0021$) expression incorporated was the highest (Fig. 3C). To study the impact of intestinal microbiota on the inflammaging status in patients with aCSVD, we analyzed the correlation of their inflammaging marker expression and commensal

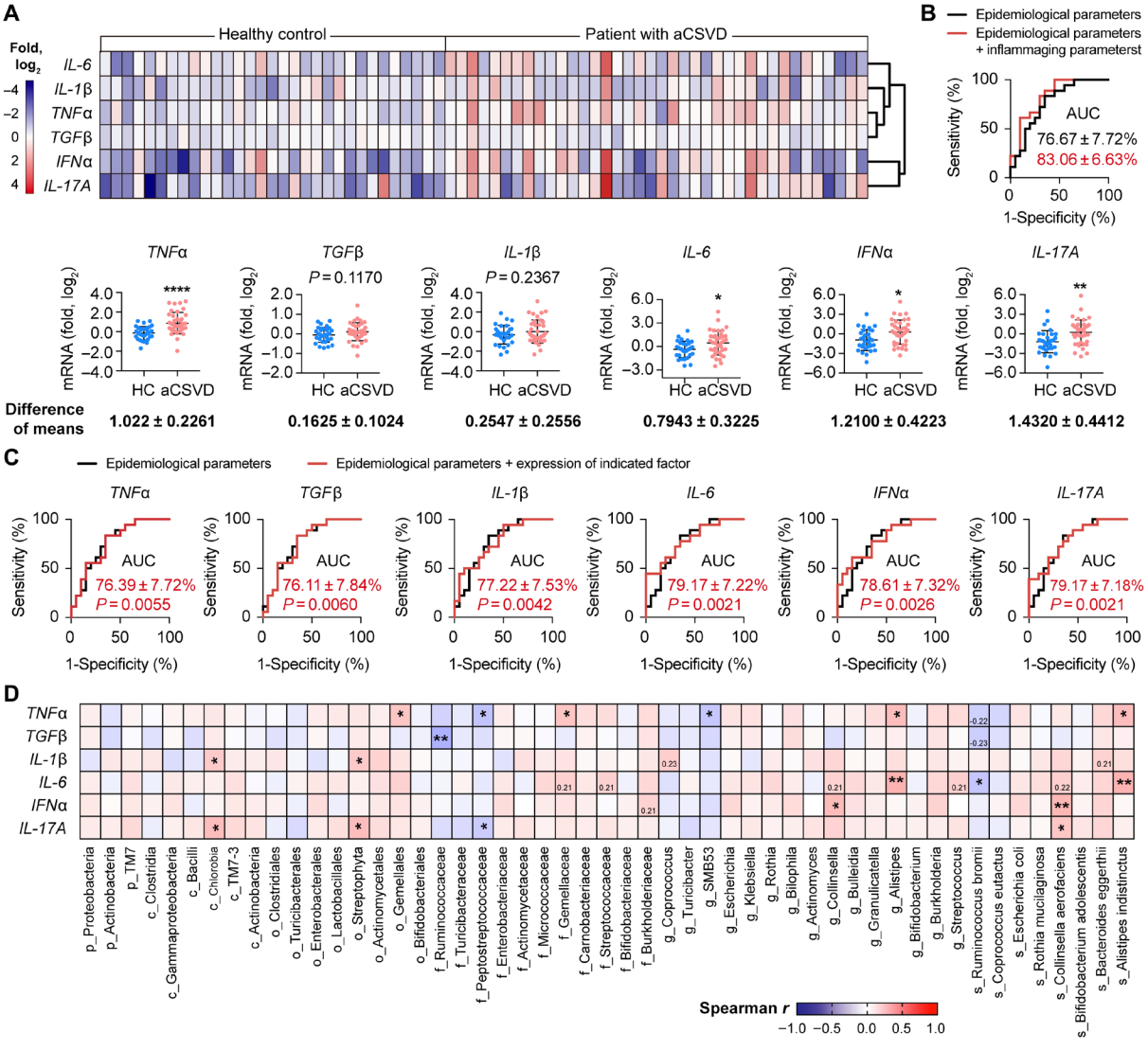

Fig. 3. Inflammaging status in patients with aCSVD and its correlation with the altered gut microbiota. (**A**) Expression of inflammaging markers. Top: Heatmap showing the mRNA level (fold, log_2). Bottom: Comparison of inflammaging marker expression in HCs ($N = 31$) and patients with aCSVD ($N = 38$). $^*P < 0.05$, $^{**}P < 0.01$, and $^{****}P < 0.0001$; by Student's t test (mean ± SD). Difference of means (±SE) is displayed. (**B**) ROC analysis of the predicting efficacy for aCSVD burden = 2 to 4 when including epidemiological characteristics (black curve, black characters) or epidemiological characteristics together with mRNA expression (delta CT log_2) of all tested cytokines (red curve, red characters). (**C**) ROC analysis of the predicting efficiency for aCSVD burden = 2 to 4 when including epidemiological characteristics alone (black curve, black characters) or together with each indicated cytokine (red curve, red characters). $N = 20$ in patients with aCSVD with burden = 0 to 1, and $N = 18$ in patients with aCSVD with burden = 2 to 4. (**D**) Association of the altered gut bacterial composition (relative abundance of gut microbiota with LDA score >2) and expression of inflammaging markers (delta CT log_2 compared with the CT value of β-*ACTIN* in RT-PCR). $N = 38$ in patients with aCSVD, and $N = 31$ in HCs. $^*P < 0.05$ and $^{**}P < 0.01$. The r values ~0.25 are also displayed.

gut microbiota composition. We documented that the mRNA level of all the tested inflammaging markers was correlated with the gut bacterial composition (defined as relative abundance of bacterial taxa with LDA score >2) (Fig. 3D). Our data are consistent with our hypothesis that gut microbiota dysbiosis may accelerate the pace of inflammaging and may promote the development and progression of aCSVD. It is worth emphasizing that among all the tested inflammaging markers, expression of *IL-17A* displayed the largest difference between patients with aCSVD and HCs and was of the highest prognostic value for detrimental imageology sign (aCSVD burden = 2 to 4), which indicated that IL-17A is of vital significance in aCSVD pathophysiology.

Microbiota of patients with aCSVD facilitate IL-17A production by neutrophils

According to the study design (Fig. 1A), we next addressed the cellular source of IL-17A in patients with aCSVD. It is reported that IL-17A could be derived from T cells, neutrophils, macrophages, dendritic cells, etc. (*20*). Therefore, we assessed IL-17A expression in the mentioned immune cells with flow cytometry. Gating strategy is illustrated in fig. S5A. In accordance with the RT-PCR data, flow cytometric analysis reported increased IL-17A expression in peripheral leukocytes of patients with aCSVD (newly recruited, $N = 14$) compared with the age-matched HCs (newly recruited, $N = 6$) (Fig. 4A). Notably, mean fluorescence intensity (MFI) of IL-17A, which revealed

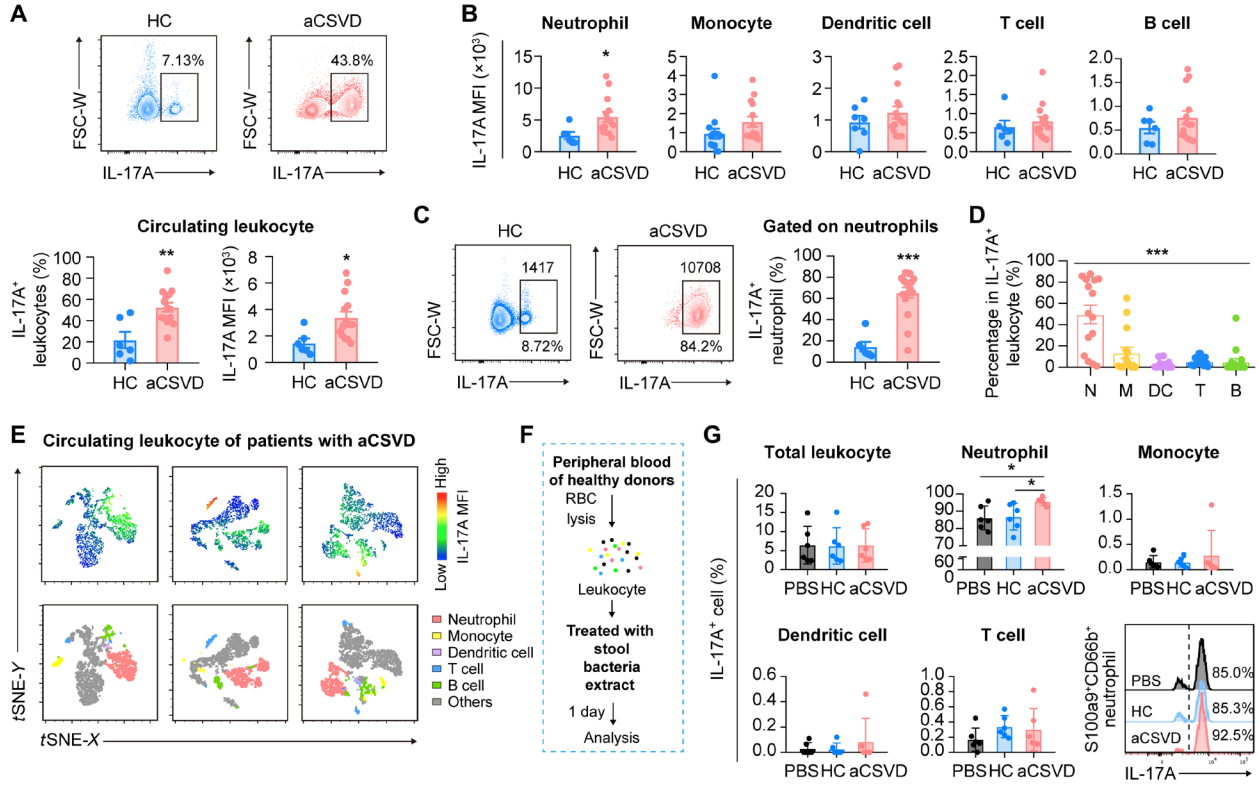

Fig. 4. Cellular source of elevated IL-17A in circulating leukocytes of patients with aCSVD. Expression of IL-17A in the circulating leukocyte of patients with aCSVD ($N = 14$) and HCs ($N = 6$) was assessed with fluorescence-activated cell sorting (FACS). (**A**) Comparison of IL-17A expression in the two groups. $^*P < 0.05$ and $^{**}P < 0.01$. FSC-W, forward scatter–width. (**B**) MFI of IL-17A in neutrophil (CD66b$^+$), monocyte (CD14$^+$), dendritic cell (CD11c$^+$), T cell (CD3$^+$), and B cell (CD19$^+$). $^*P < 0.05$. (**C**) Comparison of the frequency of IL-17A$^+$ neutrophils between the two groups. $^{***}P < 0.001$, by Student's *t* test (mean ± SEM). (**D**) Comparison of the frequency of neutrophil (N), monocyte (M), dendritic cell (DC), T cell (T), and B cell (B) among IL-17A$^+$ leukocyte in patients with aCSVD. $^{***}P < 0.001$. (**E**) Representative *t*SNE plots of the cellular source of IL-17A from three patients with aCSVD. (**F**) Experimental design of ex vivo experiments. Leukocytes were isolated from six healthy donors and treated with the fecal bacterial compounds (1 μg/ml) of patients with aCSVD or HCs. RBC, red blood cell. (**G**) IL-17A expression in total leukocyte, neutrophil (S100a9$^+$CD66b$^+$), monocyte (CD14$^+$), dendritic cell (CD11c$^+$) and T cell (CD3$^+$) at 1 day. $^*P < 0.05$, by one-way ANOVA (mean ± SD).

the average level of IL-17A protein in the gated cells, increased in circulating neutrophils (CD66b$^+$) but not in monocytes (CD14$^+$), dendritic cells (CD11c$^+$), T cells (CD3$^+$), or B cells (CD19$^+$) of patients with aCSVD compared with HCs (Fig. 4B). Accordingly, the percentage of IL-17A–expressing neutrophil elevated in patients with aCSVD (Fig. 4C). Moreover, it was neutrophil, rather than T cell or other immune players, that took up the largest proportion of IL-17A–producing leukocyte (49.68 ± 8.705%) in patients with aCSVD (Fig. 4D). As was assessed with *t*-stochastic neighbor embedding (tSNE) analysis, we revealed that IL-17A expression in neutrophil surpassed other immune cells (Fig. 4E).

The pathophysiological process of aCSVD is intricate. The internal interaction of the gut microbiota with the immune system, their reciprocal causation, and the subsequent impact on aCSVD progression are all perplexing. To simplify the process and obtain clues to understand how the altered intestinal microbiota modified the immune system in aCSVD, we performed ex vivo experiments. Total bacteria were isolated from fecal samples of patients with aCSVD and age-matched HCs. Extracts of fecal bacteria were prepared according to the methodology described previously (*21*). Circulating leukocytes were isolated from six healthy donors (three females, age = 31.00 ± 4.000; three males, age = 25.67 ± 2.082) after lysis of red blood cells and exposed to the fecal bacterial compounds (Fig. 4F). After 1 day of exposure, leukocytes were subjected to flow cytometric analysis for IL-17A expression (Fig. 4G). We found that short-term stimulation of aCSVD-associated gut bacterial extracts elicited excessive IL-17A expression in CD66b$^+$S100a9$^+$ neutrophils, while no alteration of IL-17A protein level in monocytes (CD14$^+$), dendritic cells (CD11c$^+$), and T cells (CD3$^+$) was observed (Fig. 4G).

In the meantime, spleen, the central immune organ, was obtained from healthy C57/Bl6 wild-type mice (6 to 8 weeks old), and splenocytes were exposed to the bacterial extracts (Fig. 5A). At 1 day after treatment, composition of immune cells among splenocytes remained largely invariant (fig. S5B). Of particular interest, aCSVD-associated gut bacterial extracts facilitated IL-17A expression of splenocytes compared with those treated with HC gut bacterial extracts or vehicle controls [phosphate-buffered saline (PBS)] as assessed with Western blot (Fig. 5B) and fluorescence-activated cell sorting (FACS) (Fig. 5C), which coincided with the up-regulated IL-17A–expressing leukocytes in patients with aCSVD. With flow cytometric analysis, we traced the source of IL-17A elicited by aCSVD-associated gut bacterial extracts (Fig. 5, D to H). Notably, neutrophils, which were labeled as Ly6G$^+$F4/80$^-$CD3$^-$CD19$^-$ cells (Fig. 5, D to G) or CD45$^+$CD11b$^+$S100a9$^+$Ly6G$^+$ cells (Fig. 5H), obtained increased IL-17A–producing capacity at 1 day after exposure to aCSVD-associated gut microbiota and accounted for the largest proportion of the IL-17A–producing

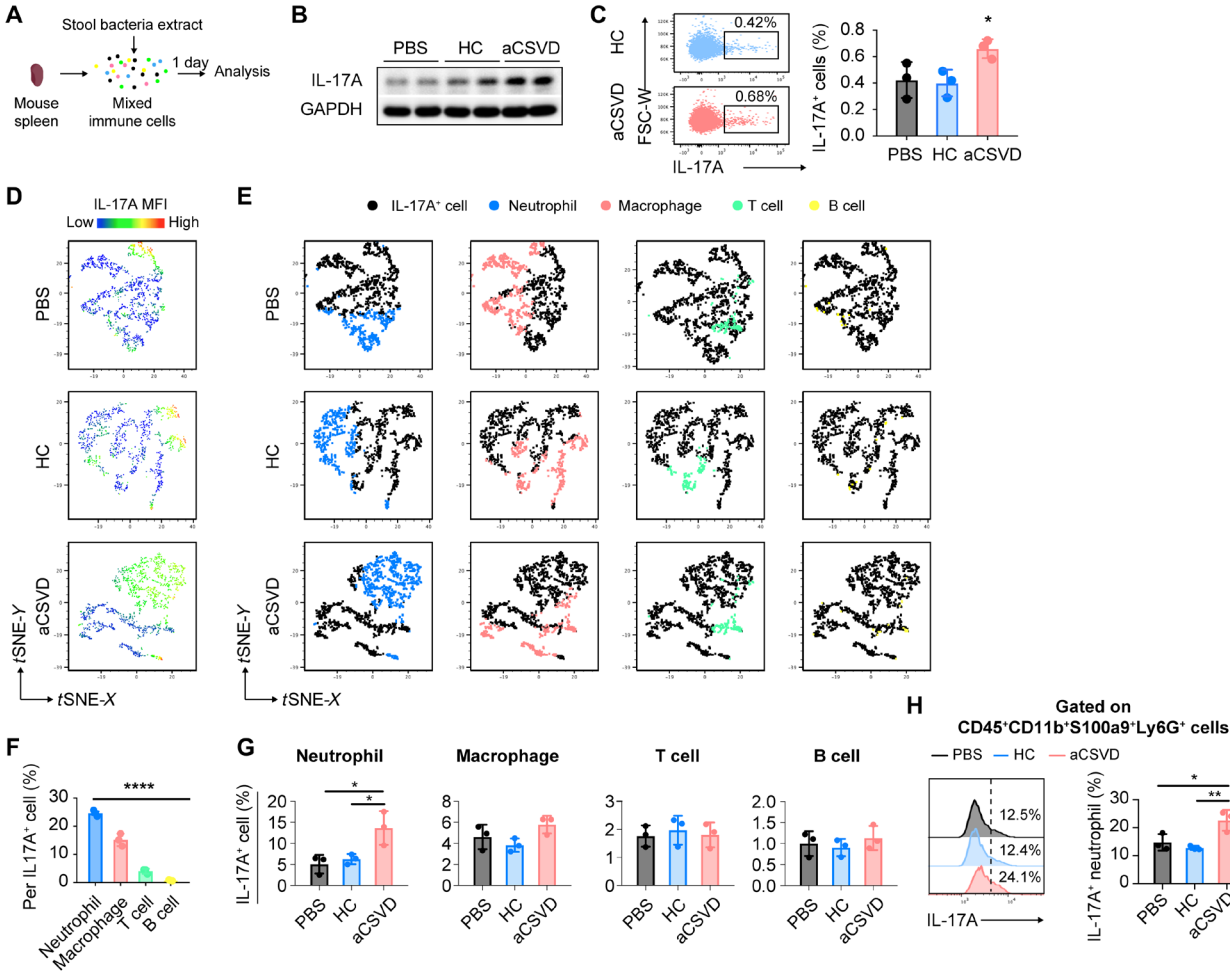

Fig. 5. Production of IL-17A by mouse splenocytes after exposure to aCSVD-associated gut bacterial extracts for 1 day. (**A**) Experimental design. Gut bacterial extracts were prepared from the fecal samples of patients with aCSVD or HCs. Splenocytes were then treated with gut bacterial extracts (1 μg/ml) or equal volume of PBS for 1 day. (**B** and **C**) Expression of IL-17A in total splenocytes at 1 day after exposure was assessed with Western blot (B) and flow cytometry (C). GAPDH, glyceraldehyde-3-phosphate dehydrogenase. (**D** and **E**) *t*SNE analysis of splenocytes with the parameters of IL-17A, Ly6G, F4/80, CD3, and CD19. (**D**) Representative *t*SNE plots of the splenocytes scaled on IL-17A expression. (**E**) Location of neutrophils (Ly6G$^+$), macrophages (F4/80$^+$), T cells (CD3$^+$), and B cells (CD19$^+$) among splenocytes. (**F**) Frequencies of the tested immune cells among L17A$^+$ splenocytes after exposure to aCSVD-associated gut bacterial extracts. (**G**) Percentages of IL-17A$^+$ cell among the tested immune cells after exposure to gut bacterial extracts. (**H**) FACS analysis of IL-17A expression in CD45$^+$CD11b$^+$S100a9$^+$Ly6G$^+$ neutrophils among splenocytes. Experiments were repeated for three times. *$P < 0.05$, **$P < 0.01$, and ****$P < 0.0001$, by one-way ANOVA (mean ± SD).

splenocytes (Fig. 5F). Nevertheless, no significant elevation of IL-17A level in T cells, B cells, or macrophages was observed at 1 day (Fig. 5, D to G). It is noted that at 3 days after exposure to aCSVD-associated gut bacterial extracts, expression of IL-17A was up-regulated in T cells (fig. S6, A and B). Percentages of CD4$^+$ regulatory T cells (CD3$^+$CD4$^+$FoxP3$^+$), CD8$^+$ regulatory T cells (CD3$^+$CD8$^+$CD103$^+$), cytotoxic T cells (CD3$^+$CD8$^+$Granzyme$^+$ or CD3$^+$CD8$^+$Perforin$^+$), B10 cells (CD19$^+$IL10$^+$), NKB (natural killer B) cells (CD19$^+$NK1.1$^+$), M2 macrophages (CD45$^+$F4/80$^+$CD206$^+$), and N2 neutrophils (CD45$^+$Ly6G$^+$CD206$^+$) among splenocytes after treatment with gut bacterial extracts or vehicle controls (PBS) were stable (fig. S5C).

Bacterial extracts of patients with aCSVD elicit IL-17A expression in neutrophils by activating RORγt signaling

We went on to investigate the molecular mechanisms of how the gut microbiota affected IL-17A production in immune cells. As is known, RORγt (regulator of reprogramming, isoform gamma-t) is the main enhancer of IL-17A expression, while signal transducer and activator of transcription 1 (STAT1) signaling suppresses IL-17A production and directs naïve T cells toward T helper cell 1 (T_H1) phenotype (*22*, *23*). Therefore, activation status of RORγt and STAT1 signaling in immune cells were analyzed. We recorded that aCSVD-associated gut bacterial extracts activated RORγt and STAT1 signaling simultaneously in splenocytes with Western blot (Fig. 6A) and flow cytometric analysis (Fig. 6, B and C). Meanwhile, we found that after exposure to aCSVD-associated gut bacterial extracts, RORγt expression increased in neutrophils, while the level of phosphorylated STAT1 (pSTAT1) remained at low level (Fig. 6, D and E). Inhibition of RORγt signaling with GSK2981278 (10 μM, MCE), which specifically interfered binding of RORγt to the *Il17a* DNA, reversed the effect of the bacterial extracts (Fig. 6F). The data indicated that aCSVD-associated commensal microbiota elicited IL-17A expression in neutrophil by activating RORγt signaling. In comparison, the aCSVD-associated bacterial extracts stimulated STAT1

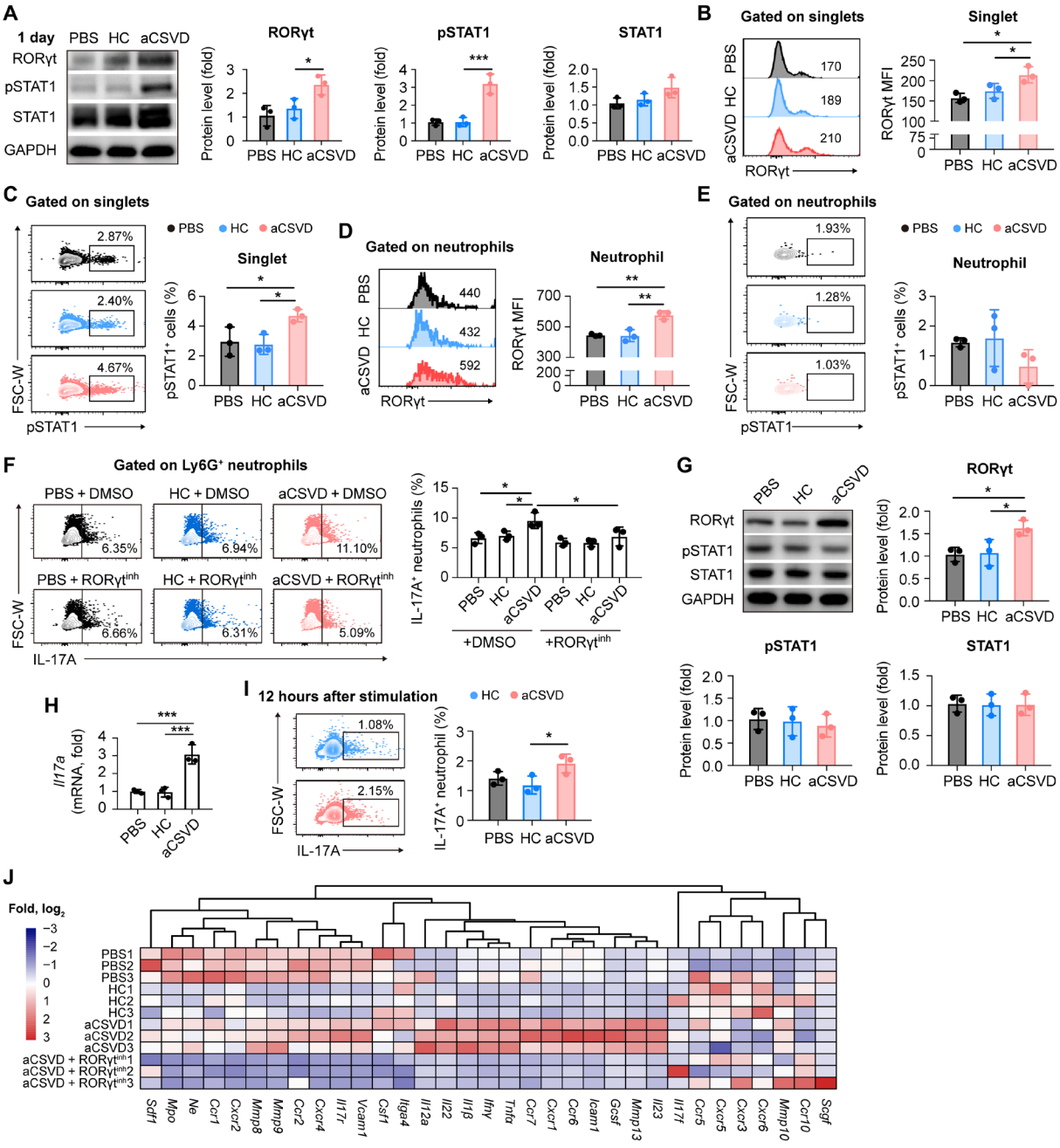

Fig. 6. RORγt signaling is activated in neutrophil after exposure to aCSVD-associated gut bacterial extracts. (**A** to **F**) Splenocytes were treated with gut bacterial extracts (1 μg/ml) for 1 day. (A) Protein level of RORγt, phosphorylated STAT1 (pSTAT1), and STAT1 as assessed with Western blot. (B to E) RORγt (B) and pSTAT1 (C) expression in singlets, RORγt (D), and pSTAT1 (E) expression in Ly6G$^+$ neutrophil measured with FACS. (F) Splenocytes were treated with gut bacterial extracts with or without RORγt inhibitor GSK2981278 (RORγt^{inh}, 10 μM) for 1 day. L-17A$^+$ neutrophil was calculated. Experiments were repeated for three times. *P < 0.05, **P < 0.01, and ***P < 0.001; by one-way ANOVA (mean ± SD). DMSO, dimethyl sulfoxide. (**G** to **J**) Bone marrow–derived neutrophils were treated with gut bacterial extracts (1 μg/ml) for 12 hours. (G) Expression of RORγt, pSTAT1, and STAT1 assessed with Western blot. (H to I) RT-PCR (H) and flow cytometric analysis (I) of IL-17A expression in neutrophils. (J) Transcriptional profile in neutrophils after exposure to bacterial extracts with or without GSK2981278 (RORγt^{inh}, 10 μM) was assessed with RT-PCR array. Statistical results are displayed in fig. S7B. Experiments were repeated for three times. *P < 0.05, **P < 0.01, and ***P < 0.001; by one-way ANOVA (mean ± SD).

signaling in T cells, which favored the T_H1 differentiation and suppressed IL-17A production (fig. S6D). In the meantime, the T_H17-associated RORγt signaling was activated in T cells, which antagonized the effect of STAT1 signaling and preserved their IL-17A expression (fig. S6C). When tipping the balance between the two signaling toward RORγt by administration of a low dose of SR0987 (2 μM, MCE), an RORγt activator, IL-17A expression in T cells significantly increased as soon as 1 day with the presence of aCSVD-associated bacterial extracts (fig. S6E). On the other hand, when introducing brain antigen in the system (10% in culture medium), IL-17A production

in T cells increased rapidly at 1 day after stimulation (fig. S6F). The results indicated that aCSVD-associated microbiota and exposure of brain antigen might synergistically activate RORγt signaling in T cells, which resulted in T_H17 differentiation and IL-17A production (fig. S6G). The presence of brain antigen showed little influence on IL-17A production in neutrophils (fig. S7A).

To confirm the impact of aCSVD-associated commensal microbiota on neutrophils, we isolated bone marrow–derived $Ly6G^+$ neutrophils with magnetic sorting and exposed the neutrophils to fecal bacterial extracts of patients with aCSVD or HCs for 12 hours due to the short life of primary cultured neutrophils. With Western blot, we found that RORγt expression increased in neutrophils, while STAT1 signaling remained stable (Fig. 6G). RT-PCR (Fig. 6H) and flow cytometric analysis (Fig. 6I) illustrated that exposure to gut bacterial extracts of patient with aCSVD increased IL-17A production in neutrophils. In the meantime, with RT-PCR array, we observed altered transcriptional profile of neutrophils after exposure to aCSVD-associated gut bacterial extracts (Fig. 6J; statistics shown in fig. S7B): (i) increased expression of proinflammatory factors. In accordance with the elevated IL-17A production, *Il17r* expression in neutrophils increased after exposure to aCSVD-associated microbiota extracts. Subsequently, mRNA level of multiple established IL-17A–associated molecules was up-regulated, including *Il12a*, *Il22*, *Ifn*γ, and *Tnf*α (*24*). Of particular interest, mRNA expression of *Il1*β and *Il23* increased, which facilitated T_H17 differentiation (*24*). (ii) Acquisition of trafficking capacity: The mRNA level of *Cxcr1* (major modulator of neutrophil trafficking), *Ccr6* (chemokine receptor for T_H17 migration), and *Ccr7* (involved in the migration of neutrophils to the lymph node) increased in neutrophils after exposure to aCSVD-associated bacterial extracts. Moreover, expression of vascular adhesion molecules, including *Icam1* and *Vcam1,* was up-regulated, indicating that neutrophils obtained the capability to infiltrate into inflamed sites. (iii) Inclination of barrier breaking: We documented that production of several MMPs elevated in neutrophils after exposure to aCSVD-associated microbiota extracts, including *Mmp8*, *Mmp9*, and *Mmp13*. Increased MMP production of neutrophils might be associated with the initial BBB injury in aCSVD pathology. Note that up-regulation of the aforementioned transcriptional profiles could be reversed by treatment of the RORγt inhibitor GSK2981278 (10 μM, MCE) (Fig. 6Jand fig. S7B). To evaluate whether leukocytes, majority of whom were neutrophils, were involved in BBB damage and obtained the capacity to infiltrate into the inflamed aCSVD lesion, we assessed the mRNA levels of *CXCR1*, *CCR6*, *CCR7*, *ICAM1*, *VCAM1*, *MMP8*, and *MMP9* in the circulating leukocytes of patients with aCSVD and HCs with RT-PCR. Consistently, we observed that circulating leukocytes of patients with aCSVD expressed higher levels of the mentioned chemokine receptors, adhesion molecules, and BBB damage-associated MMPs (fig. S7C). We thus inferred that aCSVD-associated gut microbiota activated RORγt signaling in neutrophils and endowed neutrophils with capabilities of activating the adaptive immune system, trafficking toward and infiltrating the CNS (fig. S7D).

DISCUSSION

The current study describes a previously unidentified pathophysiological mechanism for aCSVD that implicates the intestinal microbiota–immune system–brain axis, supporting the idea that aCSVD is a systemic disease rather than a focal disorder (*5*). The data suggest that gut microbiota alteration in patients with aCSVD affects the pace of inflammaging. In particular, aCSVD-associated microbiota elicits IL-17A expression in neutrophils via activating RORγt signaling. Activation of neutrophil and their increased production of IL-17A might exacerbate the systemic inflammation in patients with aCSVD.

Our study depicted altered gut microbiota composition in patients with aCSVD. On the one hand, reduced abundance of beneficial commensal microbes, such as the butyrate-producing g_Coprococcus, was observed in aCSVD-associated gut microbiota. Butyrate is one of the predominant short-chain fatty acids (SCFAs) in the gut and serves as an essential energetic source of gut epithelia (*25*). In colonocytes, SCFAs are absorbed and transported into mitochondria, where they are converted into acetyl–coenzyme A (CoA) via β-oxidation and facilitate adenosine triphosphate (ATP) production in tricarboxylic acid cycle (*25*), thus maintaining intestinal homeostasis and protecting the integrity of gut epithelium barrier (*26*). The remarkable reduction in butyrate-producing bacteria in patients with aCSVD might lead to inadequate supply of butyrate from the gut microbiota, which could subsequently result in imbalance of energetic metabolism in gut epithelia and damage of intestinal barrier. On the other hand, abundance of detrimental bacteria increased in aCSVD-associated microbiota. Expansion of potential opportunistic pathogens, including g_Escherichia, g_Klebsiella, and g_Streptococus, might provoke gut inflammation and evoke systemic inflammation. As was recorded, p_Proteobacteria, c_Gamfmaproteobacteria, o_Enterobacterales, f_Enterobacteriaceae, and g_Escherichia were correlated with total aCSVD neuroimaging burdens. p_Proteobacteria is one of the major trimethylamine (TMA) producers in the human gut (*27*). TMA is the precursor of TMAO, which is an established proatherogenic metabolite and a risk biomarker of cardio-cerebrovascular arteriosclerotic diseases (*28*, *29*). In the meantime, f_ Enterobacteriaceae has been reported to be associated with intestinal barrier dysfunction, which facilitates the entry of detrimental metabolites through the gut (*30*, *31*). Accumulation of proatherogenic metabolites and exacerbated systemic inflammation could accelerate the development of arteriolosclerosis in the pathophysiological process of aCSVD. We speculate that modifying lifestyle through multiple aspects that correct the imbalance gut microbiota composition could probably delay the progression of aCSVD, which include transferring to a fiber (butyrate)–enriched diet, as well as ensuring sufficient sleep and adequate sports.

In accordance, we recorded detrimental systemic inflammatory status in patients with aCSVD. Expression of inflammaging markers significantly elevated in the circulating leukocytes. Among the tested inflammaging mediators, IL-17A displayed the highest difference of means between HCs and patients with aCSVD. As is reported, IL-17A facilitates the production of various chemokines in the brain parenchyma, which attract infiltration of cytotoxic immune cells and promote the subsequent microvascular pathology in various neural vascular disorders (*32*–*34*). According to our data, incorporating the mRNA level of *IL-17A* in the ROC analysis for detrimental imageology signs (aCSVD burden = 2 to 4) in addition to the epidemiological parameters increased the AUC, which indicated that elevated IL-17A production in circulating leukocytes could serve as an effective alarm for poor aCSVD outcomes.

A new and unexpected finding in our study was that the most predominant cellular contributor of the increased IL-17A production in patients with aCSVD was neutrophils rather than T cells. The prominent capacity of IL-17A production in T cells and its pathogenic

role in neurovascular diseases such as ischemic stroke have been well studied (*32*, *35*). Nevertheless, we failed to document elevated IL-17A production in circulating $CD3^+$ T cells of patient with aCSVD. Moreover, aCSVD-associated bacterial extracts elicited IL-17A production in neutrophils as soon as 12 hours after stimulation, while IL-17A expression in T cells was not increased until 3 days. Introducing brain antigen into the stimulatory system advanced the IL-17A production in T cells, which indicated that antigen exposure might play a vital role in the development of IL-17A–producing T cells. It could be drainage lymph node or aCSVD lesion where T cells are equipped with the capacity of IL-17A expression with help from antigen-presenting cells. Therefore, although the frequency of $IL\text{-}17A^+$ T cells was not increased in the peripheral blood of patients with aCSVD, their pathogenic role in aCSVD could not be ruled out. Moreover, γδT cells represent another important source of IL-17A. Contribution of γδT cells in aCSVD pathology should not be neglected. On the other hand, we observed that gut bacterial extracts of patients with aCSVD activated STAT1 signaling in T cells, which was responsible for T_H1 differentiation. The findings resemble that in multiple sclerosis (MS) pathophysiology (*21*). The observation supports the notion that commonality of MS and aCSVD pathophysiology exists (*6*). The intricate immune responses in aCSVD pathophysiology are perplexing. Innate and adaptive immune systems influence each other and synergistically contribute to aCSVD development. It is noteworthy that aCSVD-associated bacterial extracts elicited IL-23 and IL-1β secretion in neutrophils, which were reported to promote IL-17A production in T cells (*24*), indicating that neutrophils and T cells could interact with each other in gut microbiota–associated aCSVD pathophysiology.

Production of IL-17A by neutrophils and the detrimental impacts have been reported (*36*, *37*). Nevertheless, neutrophils and their capacity of IL-17A production failed to attract adequate attention in the field of aCSVD study, neglecting the abundance of their quantity and rapid reaction when encountering stimulation. We recorded that after being stimulated with gut bacterial extracts from patient with aCSVD, neutrophils timely got activated and produced IL-17A as early as 12 hours, which was independent of the presence of brain antigen. The functional activities of neutrophils have decisive impacts on the outcomes of CNS diseases. Skewing neutrophil polarity toward the arginase 1–expressing "N2" phenotype promotes inflammatory resolution (*38*), while NETs impair revascularization and exacerbate BBB damage in ischemic stroke (*39*). It has been reported that NETs could bear IL-17A and display enhanced proinflammatory property (*40*). In the pathophysiological process of aCSVD, BBB leakage results in the appearance of CNS components in the periphery, which leads to activation of peripheral immune cells when encountering the inexperienced antigen (*10*, *11*). Nevertheless, the initial step of primary BBB damage is largely unknown. IL-17A expression in neutrophils has been reported to be associated with their migration capacity (*41*–*43*). Elevated MMP production and chemokine receptor expression, which could also be elicited by aCSVD-associated bacterial extracts, might further facilitate neutrophils to break down the protecting barrier. With the aforementioned cues, we infer that dysbiosis of gut microbiota enhances the proinflammatory property of neutrophil independently, equipping neutrophil with increased IL-17A–producing capacity, migration capability, and barrier-breaking function, which play key roles in the initiation of BBB injury during the development of aCSVD and the following disease progression.

It is of interest which bacteria are the dominating inducer of IL-17A among the aCSVD-associated gut microbes. We notice that many of the bacteria that enriched in the gut microbiota of patients with aCSVD, including p_Proteobacteria (*44*, *45*), p_Actinobacteria (*46*), g_Escherichia (*47*), g_Collinsella (*48*), etc., have been reported to potently induce IL-17A expression in immune cells, suggesting that the bacteria could probably activate RORγt signaling. On the other hand, our data indicated that the relative abundance of c_Chlorobia, o_Streptophyta, and s_Collinsella aerofaciens was positively correlated with *IL-17A* mRNA level in patients' leukocytes. Therefore, we speculate that the abovementioned bacteria could cooperate with each other and synergistically induce IL-17A expression in neutrophils of patients with aCSVD. Besides, our data showed that the commensal bacteria interacted closely with each other and functioned as a whole, which indicated that besides the abovementioned bacteria, other species abnormally enriched in the gut microbiota of patients with aCSVD might participate in the induction of IL-17A production.

Multiple insurmountable difficulties existed during the research. Because of the absence of a well-established animal model of aCSVD, the current study failed to verify the detrimental impacts of neutrophils modified by aCSVD-associated gut microbiota in vivo. On the other hand, because gut microbiota functions as a whole, we used the active component extracted from the fecal samples of patients with aCSVD and HCs. Nevertheless, the metabolite profile in gut microbiota of patients with aCSVD is worth identifying, and further study relying on the functioning metabolites of gut microbiota should be pursued. Moreover, as a result of the short half-life of primary cultured neutrophils (12 hours), intervention of RORγt signaling with small or short interfering RNA was impractical. We therefore suppressed RORγt signaling with its specific inhibitor GSK2981278 (*49*, *50*), while experiments with primary cultured neutrophil from RORγt knockout or mutant mice should be accomplished in the future. On the other hand, the pathogenic role of IL-17A–expressing neutrophils should be evaluated. Further efforts to discover the far-reaching pathological mechanisms and therapeutic research in aCSVD are required.

In conclusion, multiple alterations in gut microbiota composition, inflammaging status, and their association with aCSVD outcomes have been recorded. Our findings shed new light on the implication of the intestinal microbiota–immune system–brain axis in aCSVD development, indicating that lifestyle modification to reshape gut microbiota could help to orchestrate inflammatory status, thus benefitting aCSVD prevention or treatment.

MATERIALS AND METHODS

Study population

A cohort consisting of 55 patients with aCSVD was recruited to the neurology clinics in the Third Affiliated Hospital of Sun Yat-sen University from July 2018 to August 2019 consecutively. All patients recruited in the study were eligible for the inclusion criteria below: (i) with at least one arteriosclerotic risk factor, which include age >55 years, smoking (≥10 cigarettes per day for at least 10 year), BMI >28, hypertension, diabetes mellitus, impaired glucose tolerance, impaired fasting glucose, coronary heart disease, hyperlipidemia, hyperhomocysteinemia, symptomatic stroke history; (ii) with at least one common CSVD symptom including cognitive decline, gait and balance disturbance, parkinsonism, emotional or sleeping disorder,

and urinary and fecal dysfunction; (iii) MRI neuroimaging met the Standards for ReportIng Vascular changes on nEuroimaging (STRIVE) for CSVD (*51*); (iv) no visible moderate-severe intracranial arteriosclerotic stenosis in MR angiography; and (v) no ischemic stroke attributed to large cerebral artery occlusion or cardiac embolism. Patients with other CSVD etiologies secondary to genetic inheritance, infection, autoimmune inflammation, neoplasm, trauma, toxication, radiation, metabolic cerebropathy, and sporadic cerebral amyloid angiopathy were excluded. Laboratory tests and standard MRI were performed in all recruited patients for cardiovascular risk factor screening and neuroimaging assessment, respectively. A total of 62 age-matched healthy community dwellers were recruited as HCs. HCs included were defined as elderly persons without hypertension, diabetes mellitus, symptomatic stroke, or any other neurological deficits common in CSVD symptomatology and maintained normal performances in the activity of daily living (ADL) scale and mini-mental state of examination (MMSE) stratified according to educational level. Enrollment strategy is illustrated in fig. S1.

MRI protocol and neuroimaging assessment

MRI was performed on a GE 3.0-Tesla scanner MR750 (General Electric, Milwaukee, USA) with a standard eight-channel HRBRAIN coil. The MRI protocol included (i) axial T1 FLAIR (fluid-attenuated inversion recovery) weighted: repetition time (TR) = 1750 ms, echo time (TE) = 24 ms, echo train length (ETL) = 10, bandwidth (BW) = 41.67 kHz, matrix = 320 × 224, filed of view (FOV) = 240 mm, slice thickness = 5 mm, spacing = 1, and number of excitations (NEX) = 1; (ii) axial T2-weighted FrFSE (fast recovery fast spin echo): TR = 5727 ms, TE = 93 ms, ETL = 32, BW = 83.3 kHz, matrix = 512 × 512, FOV = 240 mm, slice thickness = 5 mm, spacing = 1, and NEX = 1.5; (iii) T2 FLAIR weighted: TR = 8400 ms, TE = 145 ms, inversion time (TI) = 2100 ms, BW = 83.3 kHz, flip angle (FA) = 145°, matrix = 320 × 224, FOV = 240 mm, slice thickness = 5 mm, spacing = 1, and NEX = 1; (iv) axial three-dimensional time-of-flight MR angiography (3D-TOF MRA): TR = 25 ms, TE = 3.4 ms, FA = 20°, BW = 41.67 kHz, matrix size = 384 × 320, FOV = 200 mm, slice thickness = 0.8 mm, and NEX = 1; (v) Axial T2*-weighted angiography (SWAN): TR = 77.3 ms, TE = 45 ms, BW = 62.5 kHz, FA = 15°, matrix = 384 × 320, slice thickness = 1 mm, and NEX = 1. MRI DICOM (Digital Imaging and Communications in Medicine) data were analyzed by an experienced neuroradiologist (X.C.) in ORS Visual (Montreal, Quebec, Canada). Total aCSVD neuroimaging burden was assessed according to an ordinal CSVD score (0 to 4) based on CSVD imaging principal summarized in STRIVE recommendation (*51*). One score was awarded when each of the following signs was presented: number of lacunae ≥1; number of CMBs ≥1; moderate to severe enlargement of BG-PVS (*52*); p-WMH Fazekas score 3 (extending into the deep white matter) or d-WMH Fazekas score 2 to 3 (early confluent or confluent). Cerebral atrophy was scored according to the global cortex atrophy (GCA) rating scale from 0 to 3 (0 = absent, 1 = mild, 2 = moderate, 3 = severe) (*53*).

Fecal sample collection and DNA extraction

Fresh fecal samples (~500 mg) donated by recruited patients with aCSVD or HCs were collected with genomic DNA protective solution (Longsee Biomedical Corporation, Guangzhou, China) and stored at −80°C for further high-throughput 16*S* ribosomal RNA gene amplicon sequencing.

16*S* ribosomal RNA gene amplicon sequencing

Amplification of the V3-V4 hypervariable regions of the 16*S* ribosomal RNA (rRNA) gene was performed with a high-throughput Illumina MiSeq platform. Bacterial genomic DNA was extracted from fecal samples using Fecal Microbial Genomic DNA Extraction Kit (LS-R-N-015, Longsee Biomedical Corporation, Guangzhou, China) according to the manufacturer's instructions. The V3-V4 highly variable region of 16*S* rRNA gene was amplified with sample-specific barcoded primer-forward 5′-ACTCCTACGGGAGGCAGCA-3′ and primer-reverse 5′-GGACTACHVGGGTWTCTAAT-3′ in Bio-Rad S1000 real-time fluorescence quantitative PCR system (Bio-Rad Laboratories Inc., America). The PCR protocol was as follows: (i) initial denaturation (95°C, 3 min); (ii) PCR amplification (25 cycles; 95°C, 30 s; 55°C, 30 s; 72°C, 30 s); (iii) 72°C, 5 min. After purification of PCR products, sequencing libraries were constructed on an Illumina MiSeq platform following the Illumina-recommended procedures.

Bioinformatics and biostatistics

According to the overlap between two paired-end sequences, we merged the paired-end sequences into tag and discriminated samples on the basis of the barcoded sequences. The quality of the raw sequencing data was assessed using Fast V.0.11.2, followed by sequencing reads trimming and filtering with Trimmomatic v.0.32. The sequencing adapters, three leading, three trailing bases (Phred score <Q3), and low-quality bases (Phred score <Q20) were all trimmed. Downstream sequence analysis was performed with Qualitative Insights into Microbial Ecology (QIIME 2, v.2017.12). Paired-end chimera free sequences were jointed and clustered into OTUs. Extracted representative sequences with a distance-based similarity of 99% against reference sequences in Greengenes 13_8 were assigned to clustered OTU.

Alpha diversity was estimated by calculating the Chao1 richness, observed OTU, Pielou *E* value, Faith's PD, Shannon-Wiener diversity index, and Simpson diversity index from different perspectives, which focus on the microbial community abundance and evenness. Beta diversity evaluates divergence among microbial communities based on measuring the distance matrix of dissimilarity. In this study, principal components analysis was performed to access variance among different communities. The LEfSe pipeline was used to differentially identify microbes that distinguish patients with aCSVD from HCs. The significant taxa (from phylum to species) with LDA score >2.0 indicative of dominant relative abundance are demonstrated in a stack bar-chart plot.

Quantitative determination of mRNA expression

Total RNA from cells was extracted with a commercial kit (Tiagen, China) according to the manufacturer's instructions. A total of 1 μg of RNA [$OD_{260\,nm/280\,nm}$ (optical density at 260 nm/280 nm) =1.8 to 2.2] was applied to the first-strand complementary DNA (cDNA) synthesis in a 40-μl system using PrimeScript RT reagent kit (Takara). RT-PCR was performed on a QuantStudio 5 (ABI) quantitative PCR machine using TB green Premix Ex Taq kit (Takara) with 1 μl of the synthesized cDNA in each reaction with addition of ROX. The following program was performed: 95°C for 30 s; 95°C for 5 s and 60°C for 34 s, repeated for 40 cycles; 95°C for 15 s, 60°C for 1 min, and 95°C for 15 s (melt curve). Primers used in the study are listed in table S3. In the data analysis of Fig. 3 and figs. S4 and S7C, delta CT (compared with the CT value of β-*ACTIN*) was calculated. The values of $2^{(-\text{delta CT})}$ were normalized to the means of HCs and then

subjected to $\log_2$ transformation when nonconformity with normal distribution existed (fold, $\log_2$). The mRNA expression level was visualized with a heatmap and clustered with the software of R using the "pheatmap" package. The function of "scale" was applied for value normalization. In the data analysis in Fig. 6, delta CT $\log_2$ (compared with the CT value of *GAPDH*) was visualized with a heatmap and clustered with the software of R using the pheatmap package. The function of scale was applied for value normalization. In Fig. 6, delta CT $\log_2$ of each target was normalized to mRNA expression of the PBS group (interpreted as fold change), and comparison between groups was performed with one-way analysis of variance (ANOVA).

Mixed immune cell isolation from spleen

The spleen, the central immune organ, was separated from healthy wild-type C57/Bl6 mouse (age = 6 to 8 weeks). After lysis of red blood cells, the splenocytes were washed with PBS and seeded into plates. The medium of RPMI 1640 + 10% fetal bovine serum (FBS) was used in splenocyte culture.

Neutrophil isolation from bone marrow

Primary neutrophil-enriched cultures were prepared from bone marrow of healthy wild-type C57/Bl6 mouse (age = 6 to 8 weeks). Bone marrow cells were labeled with anti-Ly6G-biotin–conjugated antibodies (BioLegend) and then subjected to incubation with anti-biotin microbeads (Miltenyi Biotec) in Hanks' balanced salt solution according to the manufacturer's instructions. Neutrophils were then isolated with a magnetic sorting machine (autoMACS, Miltenyi Biotec). The medium of RPMI 1640 + 10% FBS was used in neutrophil culture.

Preparation of gut bacterial extracts

Gut bacterial extracts were prepared according to the methodology described previously (*21*). Briefly, 0.5 mg of fecal sample was collected from patients with aCSVD or HCs and suspended in 1.5 ml of PBS. Suspension was passed through a 40-μm strainer for three times and washed with 1.5 ml of PBS twice with centrifugation (8300*g*, 5 min). The sample was then resuspended with 200 μl of PBS with protease inhibitor (Roche) and phosphatase inhibitor (Roche). After incubation in a water bath (65°C, 1 hour) to inactivate the bacteria, the sample was sonicated for 10 min. Protein concentration in the sample was then assessed. For immune cell stimulation, bacterial extract (1 μg/ml) was applied to the culture system.

Preparation of brain antigen

Brain tissue was extracted from healthy wild-type C57/Bl6 mouse (age = 6 to 8 weeks) after PBS perfusion. Brain tissue was then digested with 1 ml of 0.25% trypsin-EDTA for 20 min. Digestion was arrested with the addition of 2.5 ml of culture medium (RPMI 1650 + 10% FBS). Brain lysis was then subjected to centrifugation (4000*g*, 30 min). Supernatant was collected and pressed through a filter (pore size = 0.22 μm). Brain antigen was applied to the culture system with a ratio of antigen:culture medium = 1:9.

Flow cytometric analysis (FACS)

A total of 2 ml of peripheral blood was obtained from patients or HCs with EDTA-coated tube. After red blood cell lysis, cell suspensions were adjusted to a density of 1×10^6 cells in 100 μl of medium (RPMI 1640 with 10% FBS) and stimulated with phorbol 12-myristate 13-acetate (PMA) and ionomycin with brefeldin A for 4 hours at 37°C. Cells were then stained with appropriate antibodies for surface markers (room temperature, 15 min). The following antibodies were used for extracellular staining: CD66b (clone G10F5, 0.5 ng/μl), CD14 (clone 63D3, 0.5 ng/μl), CD3 (clone HIT3a, 0.5 ng/μl), CD19 (clone 4G7, 0.5 ng/μl), and CD11c (clone 3.9, 0.5 ng/μl) from BioLegend. For intracellular staining, cells were fixed and permeabilized using fixation and permeabilization buffers from Invitrogen following the manufacturer's instructions. Cells were then stained with appropriated antibodies in permeabilization buffer overnight (4°C). The following antibodies were used: IL-17A (BL168, 1 ng/ml). For FACS in mouse splenocytes, cells were collected, stimulated, and labeled with similar process detailed above. Mouse neutrophils were not stimulated because of short half-life, while the labeling process was similar. The following extracellular antibodies were used: Ly6G (clone 1A8, 0.5 ng/μl), F4/80 (clone BM8, 0.5 ng/μl), CD3 (clone 17A2, 0.5 ng/μl), and CD19 (clone 1D3/CD19, 0.5 ng/μl) from BioLegend. The following intracellular antibodies were applied: IL-17A (clone eBio17B7, 1 ng/ml), FoxP3 (clone FJK-16S, 1 ng/ml), perforin (clone eBioOMAK-D, 1 ng/ml), granzyme B (clone GB12, 1 ng/ml), RORγt (clone AFKJS-9, 1 ng/ml), and phospho-STAT1-Ser^{727} (clone Stat1S727-C6, 1 ng/ml) from Invitrogen (eBioscience). Isotype controls were used to establish compensation and gating parameters. For staining of S100a9 (ProteinTech, polyclonal, from rabbit, 0.5 ng/ml), first antibodies were stained overnight (4°C), followed by incubation with the secondary antibodies of anti-rabbit BV421 (BioLegend, 1:1000) for 15 min. Cells were then washed and analyzed with a flow cytometer (BD Biosciences), and the data were analyzed using the software FlowJo 10.4 (with *t*SNE plugins). The *t*SNE analysis was performed automatically by the FlowJo software with indicated parameters.

Western blot

Protein of splenocytes or neutrophils was extracted with radioimmunoprecipitation assay lysis buffer (Sigma-Aldrich). A total amount of 40 μg of protein of each sample was applied to Western blot experiments. Western blot was performed with standard SDS–polyacrylamide gel electrophoresis method and enhanced chemiluminescence detection reagents (Invitrogen). The following primary antibodies were used: STAT1 (Cell Signaling Technology, clone: D1K9Y, 1:500), phospho-STAT1 (Ser^{727}, Cell Signaling Technology, clone: D3B7, 1:500), RORγt (Abcam, clone: EPR20006, 1:1000), IL-17A (Abcam, polyclonal, 1:1000), and glyceraldehyde-3-phosphate dehydrogenase (GAPDH) (Cell Signaling Technology, clone: D16H11, 1:3000). Immunoreactivity was assessed with ImageJ (National Institutes of Health).

Statistical analysis

Test of normality was performed before the parametric analysis of Student's *t* test and one-way ANOVA. Student's *t* test: Unpaired parametric *t* test (two-tailed) was performed in data comparison of two groups in Prism7. Error bar represents SD. One-way ANOVA: No matching or pairing ANOVA was performed in data comparison of three groups or more in Prism7. Result was corrected for multiple comparisons using statistical hypothesis testing (Dunnett). Error bar represents SD. ROC analysis: In the current study, ROC analysis has been used to evaluate whether including relative abundance of gut microbiota, and/or the level of inflammaging markers, in addition to the usually used epidemiological characteristics parameters could increase the distinguishing efficacy for alarming moderate-severe aCSVD (burden = 2 to 4). Binary logistic regression was performed with the dependent parameter of grouping (two groups, aCSVD

burden = 0 to 1 as false positives, and aCSVD burden = 2 to 4 as true positives) with the indicated covariates in SPSS. Probabilities were calculated in SPSS and subjected to Prism7 for ROC curve description. Spearman correlation: Correlation between every pair of datasets was computed with Pearson correlation coefficients. The value of r was visualized with heatmap in Prism7. Expression level of mRNA was interpreted as delta CT $\log_2$ in Spearman correlation analysis.

Study approval

The clinical and the animal experimental studies were approved by the Medical Ethics Committee of the Third Affiliated Hospital of Sun Yat-sen University and the Animal Care and Use Committee of Sun Yat-sen University, respectively. All participants had been given the informed consent according to the principles illustrated in the Declaration of Helsinki.

SUPPLEMENTARY MATERIALS

Supplementary material for this article is available at http://advances.sciencemag.org/cgi/content/full/7/4/eabe4827/DC1

View/request a protocol for this paper from *Bio-protocol*.

REFERENCES AND NOTES

1. A. Mishra, G. Chauhan, M.-H. Violleau, D. Vojinovic, X. Jian, J. C. Bis, S. Li, Y. Saba, B. Grenier-Boley, Q. Yang, T. M. Bartz, E. Hofer, A. Soumaré, F. Peng, M.-G. Duperron, M. Foglio, T. H. Mosley, R. Schmidt, B. M. Psaty, L. J. Launer, E. Boerwinkle, Y. Zhu, B. Mazoyer, M. Lathrop, C. Bellenguez, C. M. Van Duijn, M. A. Ikram, H. Schmidt, W. T. Longstreth Jr., M. Fornage, S. Seshadri, A. Joutel, C. Tzourio, S. Debette, Association of variants in HTRA1 and NOTCH3 with MRI-defined extremes of cerebral small vessel disease in older subjects. *Brain* **142**, 1009–1023 (2019).
2. C. Brayne, The elephant in the room - healthy brains in later life, epidemiology and public health. *Nat. Rev. Neurosci.* **8**, 233–239 (2007).
3. L. Pantoni, Cerebral small vessel disease: From pathogenesis and clinical characteristics to therapeutic challenges. *Lancet Neurol.* **9**, 689–701 (2010).
4. G. Faraco, D. Brea, L. Garcia-Bonilla, G. Wang, G. Racchumi, H. Chang, I. Buendia, M. M. Santisteban, S. G. Segarra, K. Koizumi, Y. Sugiyama, M. Murphy, H. Voss, J. Anrather, C. Iadecola, Dietary salt promotes neurovascular and cognitive dysfunction through a gut-initiated TH17 response. *Nat. Neurosci.* **21**, 240–249 (2018).
5. A. ter Telgte, E. M. C. van Leijsen, K. Wiegertjes, C. J. M. Klijn, A. M. Tuladhar, F.-E. de Leeuw, Cerebral small vessel disease: From a focal to a global perspective. *Nat. Rev. Neurol.* **14**, 387–398 (2018).
6. Y. Fu, Y. Yan, Emerging role of immunity in cerebral small vessel disease. *Front. Immunol.* **9**, 67 (2018).
7. M. P. Noz, A. ter Telgte, K. Wiegertjes, L. A. B. Joosten, M. G. Netea, F.-E. de Leeuw, N. P. Riksen, Trained immunity characteristics are associated with progressive cerebral small vessel disease. *Stroke* **49**, 2910–2917 (2018).
8. A. F. Costa, M. Zambrano, O. H. Del Brutto, Relationship between the neutrophil-to-lymphocyte ratio and silent cerebral small vessel disease in community-dwelling older adults. The Atahualpa Project. *Geriatr. Gerontol. Int.* **17**, 2637–2639 (2017).
9. W. Walz, F. S. Cayabyab, Neutrophil infiltration and matrix metalloproteinase-9 in lacunar infarction. *Neurochem. Res.* **42**, 2560–2565 (2017).
10. B. Engelhardt, R. O. Carare, I. Bechmann, A. Flügel, J. D. Laman, R. O. Weller, Vascular, glial, and lymphatic immune gateways of the central nervous system. *Acta Neuropathol.* **132**, 317–338 (2016).
11. D. Kaiser, G. Weise, K. Möller, J. Scheibe, C. Pösel, S. Baasch, M. Gawlitza, D. Lobsien, K. Diederich, J. Minnerup, A. Kranz, J. Boltze, D.-C. Wagner, Spontaneous white matter damage, cognitive decline and neuroinflammation in middle-aged hypertensive rats: An animal model of early-stage cerebral small vessel disease. *Acta Neuropathol. Commun.* **2**, 169 (2014).
12. D. Zhang, P. S. Frenette, Cross talk between neutrophils and the microbiota. *Blood* **133**, 2168–2177 (2019).
13. A. J. Dicker, M. L. Crichton, E. G. Pumphrey, A. J. Cassidy, G. Suarez-Cuartin, O. Sibila, E. Furrie, C. J. Fong, W. Ibrahim, G. Brady, G. G. Einarsson, J. S. Elborn, S. Schembri, S. E. Marshall, C. N. A. Palmer, J. D. Chalmers, Neutrophil extracellular traps are associated with disease severity and microbiota diversity in patients with chronic obstructive pulmonary disease. *J. Allergy Clin. Immunol.* **141**, 117–127 (2018).
14. L. Liberale, F. Montecucco, J.-C. Tardif, P. Libby, G. G. Camici, Inflamm-ageing: The role of inflammation in age-dependent cardiovascular disease. *Eur. Heart J.* **41**, 2974–2982 (2020).
15. A. Schuldt, T. Assmann, M. Brezzi, F. Buscot, D. Eichenberg, J. Gutknecht, W. Härdtle, J.-S. He, A.-M. Klein, P. Kühn, X. Liu, K. Ma, P. A. Niklaus, K. A. Pietsch, W. Purahong, M. Scherer-Lorenzen, B. Schmid, T. Scholten, M. Staab, Z. Tang, S. Trogisch, G. von Oheimb, C. Wirth, T. Wubet, C.-D. Zhu, H. Bruelheide, Biodiversity across trophic levels drives multifunctionality in highly diverse forests. *Nat. Commun.* **9**, 2989 (2018).
16. T. J. Schuijt, J. M. Lankelma, B. P. Scicluna, F. de Sousa e Melo, J. J. T. H. Roelofs, J. D. de Boer, A. J. Hoogendijk, R. de Beer, A. de Vos, C. Belzer, W. M. de Vos, T. van der Poll, W. J. Wiersinga, The gut microbiota plays a protective role in the host defence against pneumococcal pneumonia. *Gut* **65**, 575–583 (2016).
17. L. Müller, S. Di Benedetto, G. Pawelec, The immune system and its dysregulation with aging. *Subcell. Biochem.* **91**, 21–43 (2019).
18. C. Franceschi, P. Garagnani, P. Parini, C. Giuliani, A. Santoro, Inflammaging: A new immune-metabolic viewpoint for age-related diseases. *Nat. Rev. Endocrinol.* **14**, 576–590 (2018).
19. L. Ferrucci, E. Fabbri, Inflammageing: Chronic inflammation in ageing, cardiovascular disease, and frailty. *Nat. Rev. Cardiol.* **15**, 505–522 (2018).
20. D. J. Cua, C. M. Tato, Innate IL-17-producing cells: The sentinels of the immune system. *Nat. Rev. Immunol.* **10**, 479–489 (2010).
21. E. Cekanaviciute, B. B. Yoo, T. F. Runia, J. W. Debelius, S. Singh, C. A. Nelson, R. Kanner, Y. Bencosme, Y. K. Lee, S. L. Hauser, E. Crabtree-Hartman, I. K. Sand, M. Gacias, Y. Zhu, P. Casaccia, B. A. C. Cree, R. Knight, S. K. Mazmanian, S. E. Baranzini, Gut bacteria from multiple sclerosis patients modulate human T cells and exacerbate symptoms in mouse models. *Proc. Natl. Acad. Sci. U.S.A.* **114**, 10713–10718 (2017).
22. Y. Yamazaki, M. Yamada, T. Kawai, T. Morio, M. Onodera, M. Ueki, N. Watanabe, H. Takada, S. Takezaki, N. Chida, I. Kobayashi, T. Ariga, Two novel gain-of-function mutations of STAT1 responsible for chronic mucocutaneous candidiasis disease: Impaired production of IL-17A and IL-22, and the presence of anti-IL-17F autoantibody. *J. Immunol.* **193**, 4880–4887 (2014).
23. L. Liu, S. Okada, X.-F. Kong, A. Y. Kreins, S. Cypowyj, A. Abhyankar, J. Toubiana, Y. Itan, M. Audry, P. Nitschke, C. Masson, B. Toth, J. Flatot, M. Migaud, M. Chrabieh, T. Kochetkov, A. Bolze, A. Borghesi, A. Toulon, J. Hiller, S. Eyerich, K. Eyerich, V. Gulácsy, L. Chernyshova, V. Chernyshov, A. Bondarenko, R. María Cortés Grimaldo, L. Blancas-Galicia, I. M. Madrigal Beas, J. Roesler, K. Magdorf, D. Engelhard, C. Thumerelle, P.-R. Burgel, M. Hoernes, B. Drexel, R. Seger, T. Kusuma, A. F. Jansson, J. Sawalle-Belohradsky, B. Belohradsky, E. Jouanguy, J. Bustamante, M. Bué, N. Karin, G. Wildbaum, C. Bodemer, O. Lortholary, A. Fischer, S. Blanche, S. Al-Muhsen, J. Reichenbach, M. Kobayashi, F. E. Rosales, C. T. Lozano, S. S. Kilic, M. Oleastro, A. Etzioni, C. Traidl-Hoffmann, E. D. Renner, L. Abel, C. Picard, L. Maródi, S. Boisson-Dupuis, A. Puel, J.-L. Casanova, Gain-of-function human STAT1 mutations impair IL-17 immunity and underlie chronic mucocutaneous candidiasis. *J. Exp. Med.* **208**, 1635–1648 (2011).
24. A. M. McGinley, C. E. Sutton, S. C. Edwards, C. M. Leane, J. De Courcey, A. Teijeiro, J. A. Hamilton, L. Boon, N. Djouder, K. H. G. Mills, Interleukin-17A serves a priming role in autoimmunity by recruiting IL-1β-producing myeloid cells that promote pathogenic T cells. *Immunity* **52**, 342–356.e6 (2020).
25. G. A. Ewy, A. B. Sanders, K. B. Kern, Compression-only cardiopulmonary resuscitation improves survival. *Am. J. Med.* **124**, 383–385 (2011).
26. G. Chen, X. Ran, B. Li, Y. Li, D. He, B. Huang, S. Fu, J. Liu, W. Wang, Sodium butyrate inhibits inflammation and maintains epithelium barrier integrity in a TNBS-induced inflammatory bowel disease mice model. *EBioMedicine* **30**, 317–325 (2018).
27. E. Jameson, A. C. Doxey, R. Airs, K. J. Purdy, J. C. Murrell, Y. Chen, Metagenomic data-mining reveals contrasting microbial populations responsible for trimethylamine formation in human gut and marine ecosystems. *Microb. Genom.* **2**, e000080 (2016).
28. G. G. Schiattarella, A. Sannino, E. Toscano, G. Giugliano, G. Gargiulo, A. Franzone, B. Trimarco, G. Esposito, C. Perrino, Gut microbe-generated metabolite trimethylamine-N-oxide as cardiovascular risk biomarker: A systematic review and dose-response meta-analysis. *Eur. Heart J.* **38**, 2948–2956 (2017).
29. X. S. Li, S. Obeid, R. Klingenberg, B. Gencer, F. Mach, L. Räber, S. Windecker, N. Rodondi, D. Nanchen, O. Muller, M. X. Miranda, C. M. Matter, Y. Wu, L. Li, Z. Wang, H. S. Alamri, V. Gogonea, Y.-M. Chung, W. H. W. Tang, S. L. Hazen, T. F. Lüscher, Gut microbiota-dependent trimethylamine N-oxide in acute coronary syndromes: A prognostic marker for incident cardiovascular events beyond traditional risk factors. *Eur. Heart J.* **38**, 814–824 (2017).
30. M. Schink, P. C. Konturek, E. Tietz, W. Dieterich, T. C. Pinzer, S. Wirtz, M. F. Neurath, Y. Zopf, Microbial patterns in patients with histamine intolerance. *J. Physiol. Pharmacol.* **69**, 579–593 (2018).
31. F. Lai, R. Jiang, W. Xie, X. Liu, Y. Tang, H. Xiao, J. Gao, Y. Jia, Q. Bai, Intestinal pathology and gut microbiota alterations in a methyl-4-phenyl-1,2,3,6-tetrahydropyridine (MPTP) Mouse Model of Parkinson's Disease. *Neurochem. Res.* **43**, 1986–1999 (2018).

32. C. Benakis, D. Brea, S. Caballero, G. Faraco, J. Moore, M. Murphy, G. Sita, G. Racchumi, L. Ling, E. G. Pamer, C. Iadecola, J. Anrather, Commensal microbiota affects ischemic stroke outcome by regulating intestinal γδ T cells. *Nat. Med.* **22**, 516–523 (2016).
33. D. W. Wojkowska, P. Szpakowski, A. Glabinski, Interleukin 17A promotes lymphocytes adhesion and induces CCL2 and CXCL1 release from brain endothelial cells. *Int. J. Mol. Sci.* **18**, 1000 (2017).
34. J. Zimmermann, M. Krauthausen, M. J. Hofer, M. T. Heneka, I. L. Campbell, M. Müller, CNS-targeted production of IL-17A induces glial activation, microvascular pathology and enhances the neuroinflammatory response to systemic endotoxemia. *PLOS ONE* **8**, e57307 (2013).
35. R. Sadler, V. Singh, C. Benakis, D. Garzetti, D. Brea, B. Stecher, J. Anrather, A. Liesz, Microbiota differences between commercial breeders impacts the post-stroke immune response. *Brain Behav. Immun.* **66**, 23–30 (2017).
36. H.-y. Yang, L. A. Vonk, R. Licht, A. M. G. van Boxtel, J. E. J. Bekkers, A. H. M. Kragten, S. Hein, O. P. Varghese, K. A. Howard, F. Cumhur Öner, W. J. A. Dhert, L. B. Creemers, Cell type and transfection reagent-dependent effects on viability, cell content, cell cycle and inflammation of RNAi in human primary mesenchymal cells. *Eur. J. Pharm. Sci.* **53**, 35–44 (2014).
37. A. B. Roos, S. Sethi, J. Nikota, C. T. Wrona, M. G. Dorrington, C. Sandén, C. M. T. Bauer, P. Shen, D. Bowdish, C. S. Stevenson, J. S. Erjefält, M. R. Stampfli, IL-17A and the promotion of neutrophilia in acute exacerbation of chronic obstructive pulmonary disease. *Am. J. Respir. Crit. Care Med.* **192**, 428–437 (2015).
38. M. I. Cuartero, I. Ballesteros, A. Moraga, F. Nombela, J. Vivancos, J. A. Hamilton, Á. L. Corbí, I. Lizasoain, M. A. Moro, N2 neutrophils, novel players in brain inflammation after stroke: Modulation by the PPARγ agonist rosiglitazone. *Stroke* **44**, 3498–3508 (2013).
39. L. Kang, H. Yu, X. Yang, Y. Zhu, X. Bai, R. Wang, Y. Cao, H. Xu, H. Luo, L. Lu, M.-J. Shi, Y. Tian, W. Fan, B.-Q. Zhao, Neutrophil extracellular traps released by neutrophils impair revascularization and vascular remodeling after stroke. *Nat. Commun.* **11**, 2488 (2020).
40. E. Frangou, A. Chrysanthopoulou, A. Mitsios, K. Kambas, S. Arelaki, I. Angelidou, A. Arampatzioglou, H. Gakiopoulou, G. K. Bertsias, P. Verginis, K. Ritis, D. T. Boumpas, REDD1/autophagy pathway promotes thromboinflammation and fibrosis in human systemic lupus erythematosus (SLE) through NETs decorated with tissue factor (TF) and interleukin-17A (IL-17A). *Ann. Rheum. Dis.* **78**, 238–248 (2019).
41. S. Qiao, H. Zhang, X. Zha, W. Niu, J. Liang, G. Pang, Y. Tang, T. Liu, H. Zhao, Y. Wang, H. Bai, Endogenous IL-17A mediated neutrophil infiltration by promoting chemokines expression during chlamydial lung infection. *Microb. Pathog.* **129**, 106–111 (2019).
42. K. L. Flannigan, V. L. Ngo, D. Geem, A. Harusato, S. A. Hirota, C. A. Parkos, N. W. Lukacs, A. Nusrat, V. Gaboriau-Routhiau, N. Cerf-Bensussan, A. T. Gewirtz, T. L. Denning, IL-17A-mediated neutrophil recruitment limits expansion of segmented filamentous bacteria. *Mucosal Immunol.* **10**, 673–684 (2017).
43. S. Li, X. Cong, H. Gao, X. Lan, Z. Li, W. Wang, S. Song, Y. Wang, C. Li, H. Zhang, Y. Zhao, Y. Xue, Tumor-associated neutrophils induce EMT by IL-17a to promote migration and invasion in gastric cancer cells. *J. Exp. Clin. Cancer Res.* **38**, 6 (2019).
44. R. P. Sequeira, J. A. K. McDonald, J. R. Marchesi, T. B. Clarke, Commensal Bacteroidetes protect against *Klebsiella pneumoniae* colonization and transmission through IL-36 signalling. *Nat. Microbiol.* **5**, 304–313 (2020).
45. M. C. Amezcua Vesely, P. Pallis, P. Bielecki, J. S. Low, J. Zhao, C. C. D. Harman, L. Kroehling, R. Jackson, W. Bailis, P. Licona-Limón, H. Xu, N. Iijima, P. S. Pillai, D. H. Kaplan, C. T. Weaver, Y. Kluger, M. S. Kowalczyk, A. Iwasaki, J. P. Pereira, E. Esplugues, N. Gagliani, R. A. Flavell, Effector T_H17 cells give rise to long-lived T_{RM} cells that are essential for an immediate response against bacterial infection. *Cell* **178**, 1176–1188.e15 (2019).
46. Y. Kang, G. Yang, S. Zhang, C. F. Ross, M.-J. Zhu, Goji Berry modulates gut microbiota and alleviates colitis in IL-10-deficient mice. *Mol. Nutr. Food Res.* **62**, e1800535 (2018).
47. C. M. Dejea, P. Fathi, J. M. Craig, A. Boleij, R. Taddese, A. L. Geis, X. Wu, C. E. DeStefano Shields, E. M. Hechenbleikner, D. L. Huso, R. A. Anders, F. M. Giardiello, E. C. Wick, H. Wang, S. Wu, D. M. Pardoll, F. Housseau, C. L. Sears, Patients with familial adenomatous polyposis harbor colonic biofilms containing tumorigenic bacteria. *Science* **359**, 592–597 (2018).
48. J. Chen, K. Wright, J. M. Davis, P. Jeraldo, E. V. Marietta, J. Murray, H. Nelson, E. L. Matteson, V. Taneja, An expansion of rare lineage intestinal microbes characterizes rheumatoid arthritis. *Genome Med.* **8**, 43 (2016).
49. E. G. Kang, S. Wu, A. Gupta, Y.-L. von Mackensen, H. Siemetzki, J.-M. Freudenberg, W. Wigger-Alberti, Y. Yamaguchi, A phase I randomized controlled trial to evaluate safety and clinical effect of topically applied GSK2981278 ointment in a psoriasis plaque test. *Br. J. Dermatol.* **178**, 1427–1429 (2018).
50. S. H. Smith, C. E. Peredo, Y. Takeda, T. Bui, J. Neil, D. Rickard, E. Millerman, J. P. Therrien, E. Nicodeme, J. M. Brusq, V. Birault, F. Viviani, H. Hofland, A. M. Jetten, J. Cote-Sierra, Development of a topical treatment for psoriasis targeting RORγ: From bench to skin. *PLOS ONE* **11**, e0147979 (2016).
51. J. M. Wardlaw, E. E. Smith, G. J. Biessels, C. Cordonnier, F. Fazekas, R. Frayne, R. I. Lindley, J. T. O'Brien, F. Barkhof, O. R. Benavente, S. E. Black, C. Brayne, M. Breteler, H. Chabriat, C. DeCarli, F.-E. de Leeuw, F. Doubal, M. Duering, N. C. Fox, S. Greenberg, V. Hachinski, I. Kilimann, V. Mok, R. van Oostenbrugge, L. Pantoni, O. Speck, B. C. M. Stephan, S. Teipel, A. Viswanathan, D. Werring, C. Chen, C. Smith, M. van Buchem, B. Norrving, P. B. Gorelick, M. Dichgans; STandards for ReportIng Vascular changes on nEuroimaging (STRIVE v1), Neuroimaging standards for research into small vessel disease and its contribution to ageing and neurodegeneration. *Lancet Neurol.* **12**, 822–838 (2013).
52. F. N. Doubal, A. M. J. MacLullich, K. J. Ferguson, M. S. Dennis, J. M. Wardlaw, Enlarged perivascular spaces on MRI are a feature of cerebral small vessel disease. *Stroke* **41**, 450–454 (2010).
53. F. Pasquier, D. Leys, J. G. Weerts, F. Mounier-Vehier, F. Barkhof, P. Scheltens, Inter- and intraobserver reproducibility of cerebral atrophy assessment on MRI scans with hemispheric infarcts. *Eur. Neurol.* **36**, 268–272 (1996).

Acknowledgments: We show our full respect and gratitude to all the participants in the study. **Funding:** This work was supported by the grants from the Guangzhou Science and Technology Program Key Project (202007030010), the National Natural Science Foundation of China (81971110 to Z.L.), the Guangzhou Science and Technology Plan Project (201904010444 to Z.L.), the Youth Program of National Natural Science Foundation of China (81901201 to W.C.), the China Postdoctoral Science Foundation Grant (2019T120776 to W.C.), the China Postdoctoral Science Foundation Grant (2018 M643332 to W.C.), and the Science and Technology Program of Guangzhou (202002030200). **Ethics statement:** All animal experiments were approved by the Third Affiliated Hospital of Sun Yat-sen University and performed following the *Guide for the Care and Use of Laboratory Animals* and Stroke Treatment. Clinical research was approved by the ethics committee of the Third Affiliated Hospital of Sun Yat-sen University. **Author contributions:** W.C. designed and performed the experiments and drafted the manuscript. X.C. collected and analyzed the data and contributed to the experimental design. X.J.M. and H.R. collected and analyzed the data. M.H. collected the data, contributed to the experimental design, and revised the manuscript. S.X.L., T.L., J.L., B.Z., D.L., and Y.H. collected the data. P.F., J.R., C.L., J.W., X.M., Q.Z., L.L., X.Z., Y.H., S.L., Q.D., Q.T., L.A., W.L., M.Z., L.S., C.X., H.S., G.X., and K.Z. collected samples from donors and participated in the data analysis. C.L., G.X., K.Z., Z.Z., and T.C. analyzed the composition of gut microbiota. Y.L. and W.Q. revised the manuscript. Z.L. and A.P.X. designed and supervised the study and critically revised the manuscript. All authors read and approved the final manuscript. **Competing interests:** The authors declare that they have no competing interests. **Data and materials availability:** All data needed to evaluate the conclusions in the paper are present in the paper and/or the Supplementary Materials. Additional data related to this paper may be requested from the authors.

Submitted 24 August 2020
Accepted 3 December 2020
Published 22 January 2021
10.1126/sciadv.abe4827

Citation: W. Cai, X. Chen, X. Men, H. Ruan, M. Hu, S. Liu, T. Lu, J. Liao, B. Zhang, D. Lu, Y. Huang, P. Fan, J. Rao, C. Lei, J. Wang, X. Ma, Q. Zhu, L. Li, X. Zhu, Y. Hou, S. Li, Q. Dong, Q. Tian, L. Ai, W. Luo, M. Zuo, L. Shen, C. Xie, H. Song, G. Xu, K. Zheng, Z. Zhang, Y. Lu, W. Qiu, T. Chen, A. P. Xiang, Z. Lu, Gut microbiota from patients with arteriosclerotic CSVD induces higher IL-17A production in neutrophils via activating RORγt. *Sci. Adv.* **7**, eabe4827 (2021).

ScienceAdvances

Gut microbiota from patients with arteriosclerotic CSVD induces higher IL-17A production in neutrophils via activating ROR#t

Wei CaiXiaodong ChenXuejiao MenHengfang RuanMengyan HuSanxin LiuTingting LuJinchi LiaoBingjun ZhangDanli LuYinong HuangPing FanJunping RaoChunyan LeiJihui WangXiaomeng MaQiang ZhuLili LiXiuyun ZhuYujiao HouShu LiQing DongQing TianLulu AiWenjing LuoMengyun ZuoLiping ShenCongyan XieHongzhong SongGanlin XuKangdi ZhengZhao ZhangYongjun LuWei QiuTao ChenAndy Peng XiangZhengqi Lu

Sci. Adv., 7 (4), eabe4827. • DOI: 10.1126/sciadv.abe4827